MHD Double-diffusive Convection Flow of Hybrid Nanofluid over the Vertical Plate under Porous Medium

Palky Handique, Swapnali Doley, Susanta Maity, A. Vanav Kumar, L. Jino

***Abstract*—A study is conducted to inspect the flow characteristics of a hybrid nanofluid over a vertical plate under the influence of magnetohydrodynamic free convection by considering chemical reaction, diffusion-thermo, thermal diffusion, thermal radiation, and viscous dissipation. However, the effects of Hall current and ion-slip were neglected. The flow of a hybrid nanofluid is considered to occur in a porous medium. To describe the flow, a set of ruling governing equations is generated in conjunction with conservation laws. The derived ruling equations were non-dimensionalized using various dimensionless parameters and variables. The obtained dimensionless form of equations was then solved numerically with the help of FORTRAN algorithm. The results were retrieved in terms of velocity, temperature, concentration, Nusselt number, skin friction, and Sherwood number. Also, the study aimed to compare the heat and mass transfer behavior of various Cu-water-based hybrid nanoliquids. In this regard, Al_2O_3-Cu-water, Ag-Cu-water, MWCNT-Cu-water, and TiO_2-Cu-water hybrid nanofluid flow's heat and mass transfer rates were analyzed.**

***Index Terms*—Hybrid nanofluid, vertical plate, radiation, Soret and Dufort, chemical reaction.**

I. Introduction

THE transfer of heat by fluids plays a significant role in many applications. The demand for research on thermal energy transport is more significant due to its necessity in various fields of engineering, particularly in areas such as heat exchangers, manufacturing processes, chemical reactors, electronic components, crystal formation, nuclear reactors, plasma studies, and more [1], [2], [3], [4], [5]. For instance, Sparrow and Tien [6] determined the convection heat loss and its performance on a solar collector plate under inclination and yawing. Apart from this, a significant issue in electronic components in the previous century is due to poor thermal management. In this regard, Yeh [7] reviewed techniques and other developments to overcome the failures of electronic components due to a temperature increase. Recently, Rezaei et al. [8] investigated the effects of heat and mass transfer (HMT) on controlling the microstructures during the manufacturing process. Jino et al. [9], [10] analyzed the effect of nitrate transport during a non-isothermal state. This nitrate transport leads to non-manageable leaching of crofting runoff and effluents from fertilizers. So, it is foremost to examine the heat transfer characteristics by fluids to control the necessary calamities.

A pioneering study by Soundalgekar [11] focused on free convection over an infinite vertical plate (VP) that is moved impulsively. The study shows an increase in skin friction when the plate is heated, and there is a decrease in skin friction when the plate is cooled. Kafoussias [12] explored the heat and mass transfer (HMT) effects on VP when it is subjected to motion. From the study, it is noted that there is a rise in velocity/skin friction with the Soret number and a reduction in velocity/skin friction with the Dufort number. Hossain et al. [13] investigated the flow of dense fluid (with varying viscosity) over the porous VP under the radiative-free convection effect. It is found that the skin friction and Nusselt number undergo significant changes with varying suction, viscosity variation, and radiation parameter. Muthucumaraswamy [14] examined the role of chemical reaction while the fluid flows over the oscillating VP. The examination is carried out under the VP with variable temperature and found that the velocity declines when the chemical reaction effects are enhanced. Ghani et al. [15] explored the HMT rate during natural convective flow of fluid that passes over the inclined VP. The findings of the study show that the decrement of Prandtl number improves the velocity and temperature distribution. However, concentration increases with an increase in the Prandtl number. Rubbab et al. [16] focused on the analysis of fluid flow over a VP and its heat transfer behavior due to exponential heating and shear stress boundary. During the shear stress boundary condition, the velocity is found to be increasing when the Grashof number advances. Rani and Palli [17] focused on the effects of heat source and magnetic field during when the fluid passes a porous VP under the convection effects. The plots show that the heat source effect improves the buoyancy, and the magnetic field reduces the same. Ahmed et al. [18] explored the chemical reaction during the radiation-convection flow over the exponentially accelerated VP. The enhancement of the chemical reaction declines the fluid velocity and concentration. Umamaheswar et al. [19] studied the MHD convection flow over a porous VP (inclined) under the influence of Ohmic heating and heat generation. The findings show an increment in the Nusselt number and skin friction with the heat source effects.

Manuscript received Nov 2, 2023; revised Jul 7, 2024.

Palky Handique is a Research Scholar in the Department of Basic and Applied Science, National Institute of Technology, Jote, Arunachal Pradesh, India (e-mail: hpalky93@gmail.com)

Swapnali Doley is a Research Scholar in the Department of Basic and Applied Science, National Institute of Technology, Jote, Arunachal Pradesh, India (e-mail: swapnalidoley05@gmail.com)

Susanta Maity is an Associate Professor in the Department of Basic and Applied Science, National Institute of Technology, Jote, Arunachal Pradesh, India (e-mail: susantamaiti@gmail.com)

A. Vanav Kumar is an Associate Professor in the Department of Basic and Applied Science, National Institute of Technology, Jote, Arunachal Pradesh, India (e-mail: vanavkumar.a@gmail.com)

L. Jino is an Assistant Professor in the Department of Mechanical Engineering, Sathyabama Institute of Science and Technology, Chennai, Tamilnadu, India (Corresponding author e-mail: jinogojulee@gmail.com)

Cheng [20] studied the mixed convection effects during the fluid passing a porous VP. The study shows that the heat transfer rate improves with the enhancement of mixed convection effect. Moreover, the combination of heat source and chemical reaction effects on MHD mixed convection flow over a VP is analyzed by Seshadri and Munjam [21]. It is noted that the raise in velocity and fall in concentration when the double-diffusive convection effects are increased. In addition, it is noted that the temperature distribution enhances with the chemical reaction parameter. Agbaje et al. [22] worked on the large spectral collocation method to find the MHD free convection behavior of fluid that passes over the VP and is subjected to Soret and Dufort effects. It is found that the Dufort number reduces the heat transfer rate under the presence of radiation. Recently, Suganya et al. [23] discussed the flow patterns due to the double-diffusive MHD convection flow over an inclined VP under chemical reaction effects. There is a reduction in velocity is spotted with the increase in viscous dissipation, Schmidt number, chemical reaction, and magnetic parameter. Aravind and Ravikumar [15] investigated the radiation effect along with the HMT rate during the convection flow over the oscillating VP. The results show that the oscillating parameter, radiation, and convection parameters such as thermal and mass Grashof numbers have a significant effect on the HMT rate.

A nanofluid is a fluid containing nanometer-sized particles called nanoparticles. These fluids are highly utilized by industrialists based on their thermal conductivity and other specific properties when compared to normal/base fluids. Nanofluids are solid-liquid composite materials consisting of solid nanoparticles with sizes 1-100 nm suspended in a liquid. The nanoparticles used in nanofluids are typically made of metals, oxides, carbides, or carbon nanotubes. The term ”nanofluid” was first introduced by Choi [25], and many other researchers reported its notable behavior and properties, which are more useful than normal fluids [26], [27], [28]. RamReddy et al. [29] investigated the Soret effect on mixed convective nanofluid flow over a VP. Their investigation shows an increment in velocity with the addition of the Soret number. However, there is a reduction in temperature distribution noted with the Soret number. Ali et al. [30] analyzed the effect of variation of surface velocity/temperature/concentration on HMT when the nanofluid (Ag/TiO_2/Cu/Al_2O_3-water) passes over the VP. The analysis is done when free convection is stimulated along with the applied magnetic field. The notable results during the analysis are that the Cu-water-based nanofluid provides a higher Nusselt number, and the Ag-water-based nanofluid provides a lesser Nusselt number. Additionally, it is noted that the convection flows by nanofluids are reduced with the applied magnetic fields. Alkasasbeh et al. [31] compared the natural convective flow and heat transfer rate of water-based and kerosene nanofluid when it passes over the hot circular cylinder. Reddy et al. [32] discussed the free convective HMT flow of nanofluid when the VP is moving. Under the influence of heat source and the Soret effect, it is noticed that the temperature distribution enhances with the heat source and the volume fraction of nanoparticles. Falodun and Ayegbusi [33] explored the flow mechanism when the Soret-Dufort effects are considered to analyze the HMT rate. The analysis is done during the reactive-radiative-convective nanofluid flow over the VP. The analysis results illustrate the enhancement of velocity and temperature distribution with the radiation parameter along with a minor change in the concentration distribution. Khan et al. [34] considered the flow of Maxwell Nanofluid over the VP under ramped isothermal/solutal conditions. Flow dampening is noticed when increasing the fraction of nanoparticles in engine oil. The dampening in flow is due to viscosity. Arulmozhi et al. [35] made an HMT analysis of Cu-water nanofluid over a moving VP under reactive-radiative-convection effects under an applied magnetic field. It is noted that the convection effects due to double diffusion make the growth in the convection flow.

The inability of some properties within a water-like base fluid is reinforced by the addition of any one type of nanoparticle [36]. However, only particular types of properties that are enhanced in the nanofluid based on the properties of that specific nanoparticle. To enhance the overall properties of the base fluid, there is an option to add more than one variety of nanoparticles (i.e., hybrid nanoparticles). For instance, Suresh et al. [37] synthesized Al_2O_3-Cu-water HNF and explored its properties. It is found that the overall thermophysical properties are enhanced, and its stability mixture nature also improved. Also, from the studies of various authors, the enhancement of thermal conductivity and other properties is noted [38], [39], [40]. Bibi et al. [41] studied the free convection effects of NF or HNF on flow over the VP. The study compares the fluid flow and range of Nusselt number on NF and HNF by varying the volume fraction of NF/HNF and the power law index. Rajesh et al. [42] examined the HNF flow adjacent to the VP and its heat transfer behavior on MHD free convection effects. In addition, the effects due to heat generation and radiation on heat transfer behavior are explored. It is noted that the addition of volume fraction improves the Nusselt number, and the Radiation parameter reduces the same. At higher values of the volume fraction parameter, Al_2O_3-Cu-water HNF provides a higher Nusselt number. Following that, Al_2O_3-CuO-water HNF, Al_2O_3-Ag-water HNF, and Cu-water NF provide a higher Nusselt number. More recently, Wahid et al. [43] discussed the mixed convection flow of Al_2O_3-Cu-water HNF on VP's stagnation point. By considering the effects of Soret and Dufort, it is noted that the HMT rate increases on enhancing the mixed convection effects. Jaismitha and Sasikumar [44] compared the HMT rate of Cu-water-based HNF during the free convective flow in a channel and found that the Cu-SiO2-water HNF provides a superior heat transfer rate as compared to Cu-Al_2O_3-water, Cu-SiO2-water, and Cu-TiO_2-water HNF, respectively. Gumber et al. [45] analyzed the heat transfer of CuO-Ag-water-based micro-polar HNF when flowing past a VP under MHD-radiative-convective, heat source/sink, and viscous dissipation effects. Under these effects, it is noted that the heat transfer improves when the amount of volume fraction of HNF is ascended. With the advancement from the above studies, the current study examines the HMT rate and fluid flow of HNF over the VP. In this study, various combinations/mixtures of HNF are undertaken, and their behavior on various effects are examined.

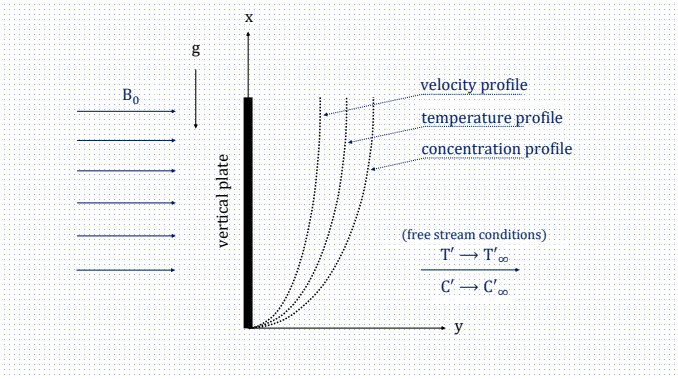

Fig. 1: Physical Problem

II. Mathematical Formulation

Considered a set of governing equations to illustrate the flow of HNF over the hot VP as depicted in Fig. 1. The equations are designed to interpret the flow of HNF over the VP by considering the VP is infinitely long such that the velocity vector signs the upward motion $\overrightarrow{V} = U(y,t)i$.

$$\rho_{HNF}\frac{\partial U}{\partial t} = \mu_{HNF}\left(\frac{\partial^2 U}{\partial y^2} - \frac{U}{K_p}\right) - \sigma B_0^2\,(U) + \left[(\rho\beta)_{HNF}\,(T-T_\infty) + (\rho\beta^*)_{HNF}\,(C-C_\infty)\right] g \tag{1}$$

$$(\rho c_p)_{HNF}\frac{\partial T}{\partial t} = k_{HNF}\left(\frac{\partial^2 T}{\partial y^2}\right) + \mu_{HNF}\left(\frac{\partial u}{\partial y}\right)^2 - \frac{\partial q_r}{\partial y} + \frac{D_m k_t}{c_s}\frac{\partial^2 C}{\partial y^2} + \left[q_0\,(T-T_\infty) + q_1\,(C-C_\infty)\right] g \tag{2}$$

$$\frac{\partial C}{\partial t} = D\left(\frac{\partial^2 C}{\partial y^2}\right) - k_r^2 C + \frac{D_m k_t}{T_m}\frac{\partial^2 T}{\partial y^2} \tag{3}$$

Here, the governing equations are derived by considering various assumptions such as

1) The HNF is assumed to be incompressible.
2) The nanoparticles within the HNF are considered to be in thermal equilibrium.
3) The size and shape of the nanoparticles are not taken into account.
4) Hall current effects are not incorporated into the model.
5) Ion-slip effects are not considered in the analysis.
6) The influence of thermal radiation flux (q_r) is included in the study.
7) The flow is subject to an applied magnetic field.
8) The model does not account for induced magnetic field effects.
9) No-slip conditions are assumed between the nanoparticles and water molecules.
10) The entire HNF flow is treated as a single-phase flow.
11) The Boussinesq approximations are applied for simplicity.
12) Viscous dissipation effects are considered in the analysis.
13) The influence of Radiation absorption effects is incorporated.
14) Thermal diffusion effects are included in the model.
15) Diffusion-thermo effects are entertained in the analysis.
16) Finally, the model include chemical reaction effects.

Apart from the assumptions, the boundaries of flow are determined as,

$$U = 0;\ T = T_\infty;\ C = C_\infty;\ t \le 0 \tag{4}$$

$$U = U_0;\ T = T_h;\ C = C_h;\ y = 0\ t > 0 \tag{5}$$

$$U{\to}0;\ T{\to}T_\infty;\ C{\to}C_\infty;\ y{\to}0;\ t > 0 \tag{6}$$

The terms with subscripts HNF in equations (1-3) illustrate the property of hybrid nanofluids which includes the combined property of water and nanoparticles. Thus the thermophysical properties of HNF are written as a function of volume fraction of each nanoparticles present in it and the following equations describe the same.

$$\mu_{HNF} = \frac{\mu_{bf}}{(1-\sum\phi_i)^{2.5}} \tag{7}$$

$$\rho_{HNF} = \rho_{bf} - \rho_{bf}\sum\phi_i + \rho_{hp}\sum\phi_i \tag{8}$$

$$(\rho c_p)_{HNF} = (\rho c_p)_{bf} - (\rho c_p)_{bf}\sum\phi_i + (\rho c_p)_{hp}\sum\phi_i \tag{9}$$

$$(\rho\beta)_{HNF} = (\rho\beta)_{bf} - (\rho\beta)_{bf}\sum\phi_i + (\rho\beta)_{hp}\sum\phi_i \tag{10}$$

$$k_{HNF} = \frac{k_{bf}\,(k_{hp} + 2k_{bf} - 2k_{bf}\sum\phi_i + 2k_{hp}\sum\phi_i)}{k_{hp} + 2k_{bf} - \ k_{bf}\sum\phi_i + k_{hp}\sum\phi_i} \tag{11}$$

$$\sigma_{HNF} = \sigma_{BF} + \frac{\sigma_{BF}\left[3\sum\phi_i\left(\left(\frac{\sigma_{HP}}{\sigma_{BF}}\right) - 1\right)\right]}{\left(\frac{\sigma_{HP}}{\sigma_{BF}}\right) + 2 - \sum\phi_i\left(\left(\frac{\sigma_{HP}}{\sigma_{BF}}\right) - 1\right)} \tag{12}$$

Where, HP in above equations denotes the hybrid particles. The property of hybrid particle is a summation of each nanoparticle. Thus it is written as,

$$\rho_{HP} = \frac{\sum(\phi)_i(\rho)_i}{\sum\phi_i} \tag{13}$$

$$\beta_{HP} = \frac{\sum(\phi)_i(\beta)_i}{\sum\phi_i} \tag{14}$$

$$\sigma_{HP} = \frac{\sum(\phi)_i(\sigma)_i}{\sum\phi_i} \tag{15}$$

$$(c_p)_{HP} = \frac{\sum(\phi)_i(c_p)_i}{\sum\phi_i} \tag{16}$$

$$k_{HP} = \frac{\sum(\phi)_i(k)_i}{\sum\phi_i} \tag{17}$$

The radioactive heat flux term in temperature equation (2) can be approached by using Rosseland approximation and is given by,

$$q_r = -\frac{4\sigma^*}{3R_c}\frac{\partial T^4}{\partial y} \tag{18}$$

where σ^* is Stefan Bolzmann constant and R_c is mean Rosseland absorption constant.

If temperature differences within the flow are sufficiently small, then q_r can be linearized by expanding T^4 into the Taylor series about T_∞ as follows:

$$T^4 = 3T_\infty^3(T-T_\infty) + 6T_\infty^2(T-T_\infty)^2 + \ldots\ldots \tag{19}$$

Neglecting higher-order terms in equation (19) takes the form

$$T^4 \cong 4T_\infty^3 T - 3T_\infty^4 \tag{20}$$

Eventually, by substituting the equation, radiative flux approximated term in equation (2) provides,

$$\begin{aligned}(\rho c_p)_{HNF}\frac{\partial T}{\partial t} &= k_{HNF}\left(\frac{\partial^2 T}{\partial y^2}\right) + \mu_{HNF}\left(\frac{\partial u}{\partial y}\right)^2 \\ &-\frac{16\sigma^* T_\infty^3}{3R_c}\left(\frac{\partial^2 T}{\partial y^2}\right) + \frac{D_m k_t}{c_s}\frac{\partial^2 C}{\partial y^2} \\ &+\left[q_0\left(T-T_\infty\right)+q_1\left(C-C_\infty\right)\right]g\end{aligned} \tag{21}$$

In order to transform the dimensional equation to dimensionless form, the following set of variables are used.

$$\tau = \frac{t u_0^2}{\nu_f} \tag{22}$$

$$\Omega = \frac{U}{U_0} \tag{23}$$

$$Y = \frac{U_0 y}{\nu_{BF}} \tag{24}$$

$$\theta = \frac{T-T_\infty}{T_h - T_\infty} \tag{25}$$

$$\Upsilon = \frac{T-T_\infty}{T_h - T_\infty} \tag{26}$$

Thus the received non-dimensionally transformed equation as,

$$\frac{\partial \Omega}{\partial \tau} = A_1\left(\frac{\partial^2 \Omega}{\partial Y^2}\right) + A_2\theta + A_3\Upsilon - A_4\Omega - A_5\Omega \tag{27}$$

$$\begin{aligned}\frac{\partial \theta}{\partial \tau} &= (A_6+A_7)\left(\frac{\partial^2 \theta}{\partial Y^2}\right) + A_8\left(\frac{\partial u}{\partial Y}\right)^2 + A_9\theta \\ &+A_{10}\Upsilon + A_{11}\left(\frac{\partial^2 \Upsilon}{\partial Y^2}\right)\end{aligned} \tag{28}$$

$$\frac{\partial \Upsilon}{\partial \tau} = A_{12}\left(\frac{\partial^2 \Upsilon}{\partial Y^2}\right) + A_{13}\left(\frac{\partial^2 \theta}{\partial Y^2}\right) - A_{14}\Upsilon \tag{29}$$

where,

$$A_1 = \frac{1}{\left(1-\sum\phi_i\right)^{2.5}\left[1-\sum\phi_i+\sum\phi_i\left(\frac{\rho_{HP}}{\rho_{BF}}\right)\right]}$$

$$A_2 = \frac{\left[1-\sum\phi_i+\sum\phi_i\left(\frac{(\rho\beta)_{HP}}{(\rho\beta)_{BF}}\right)\right]Gr}{1-\sum\phi_i+\sum\phi_i\left(\frac{(\rho)_{HP}}{(\rho)_{BF}}\right)}$$

$$A_3 = \frac{\left[1-\sum\phi_i+\sum\phi_i\left(\frac{(\rho\beta)_{HP}}{(\rho\beta)_{BF}}\right)\right]Gc}{1-\sum\phi_i+\sum\phi_i\left(\frac{(\rho)_{HP}}{(\rho)_{BF}}\right)}$$

$$A_4 = \frac{Ha}{\left[1-\sum\phi_i+\sum\phi_i\left(\frac{\rho_{HP}}{\rho_{BF}}\right)\right]}$$

$$A_5 = \frac{1}{Da}$$

$$A_6 = \left(\frac{k_{HNF}}{k_{BF}}\right)\left\{\frac{1}{Pr\ \left[1-\sum\phi_i+\sum\phi_i\left(\frac{(\rho c_p)_{HP}}{(\rho c_p)_{BF}}\right)\right]}\right\}$$

$$A_7 = \left(\frac{k_{HNF}}{k_{BF}}\right)\left\{\frac{Rd}{Pr\ \left[1-\sum\phi_i+\sum\phi_i\left(\frac{(\rho c_p)_{HP}}{(\rho c_p)_{BF}}\right)\right]}\right\}$$

$$A_8 = \frac{Ec}{\left[\left(1-\sum\phi_i\right)^{2.5}\right]\left[1-\sum\phi_i+\sum\phi_i\left(\frac{(\rho c_p)_{HP}}{(\rho c_p)_{BF}}\right)\right]}$$

$$A_9 = \frac{Q}{\left[1-\sum\phi_i+\sum\phi_i\left(\frac{(\rho c_p)_{HP}}{(\rho c_p)_{BF}}\right)\right]}$$

$$A_{10} = \frac{Q_1}{\left[1-\sum\phi_i+\sum\phi_i\left(\frac{(\rho c_p)_{HP}}{(\rho c_p)_{BF}}\right)\right]}$$

$$A_{11} = Du$$

$$A_{12} = 1/Sc$$

$$A_{13} = So$$

$$A_{14} = Rn$$

The dimensionless variable used in above parameters A_1 to A_{14} is $Ha{=}\sigma B_0^2\nu_{BF}/\rho_f U_0^2$ is the Magnetic Parameter, $Gr{=}\nu_{BF}g\beta_{BF}\left(T-T_\infty\right)/U_o^3$ is the Thermal Grashof number, $Gc{=}\nu_{BF}g\beta^*_{BF}\left(C-C_\infty\right)/U_0^3$ is the Mass Grashof number, $Da{=}KU_o^2/\nu_{BF}^2$ is the Porosity parameter, $Du{=}D_m K_T\left(C-C_\infty\right)/C_s c_p\nu_{BF}\left(T-T_\infty\right)$ is the Dufort number, $Q{=}q_0\nu_{BF}^2/U_0^2K_{BF}$ is the heat source parameter, $Q_1{=}q_1\nu_{BF}^2/U_0^2k_{BF}$ is the Radiation absorption parameter, $Rd = 16\sigma^* T_\infty^3/3R_c$ is the Radiation parameter, $Pr{=}\left(\mu c_p\right)_{BF}/k_{BF}$ is the Prandtl number, $Sc{=}\nu_{BF}/D$ is the Schmid number, $S_0{=}D_m K_T\left(T-T_\infty\right)/\nu T_m\left(C-C_\infty\right)$ is the Sorret number and $Rn = K_r^2\nu_{BF}/U_0^2$ is a chemical reaction parameter

The respective dimensionless boundaries are,

$$\Omega = 0;\ \theta = 0;\ \Upsilon = 0;\ \tau \le 0 \tag{30}$$

$$\Omega = 1;\ \theta = 1;\ \Upsilon = 1;\quad Y = 0;\ \tau > 0 \tag{31}$$

$$\Omega{\to}0;\ \theta{\to}0;\ \Upsilon{\to}0;\quad Y{\to}0;\ \tau > 0 \tag{32}$$

The effectiveness of heat/mass convection rate eover a VP is illustrated using Nusselt number, Skin friction and Sherwood number respectively.

III. Numerical Solution

To obtain numerical solutions for the Hybrid Nanofluid (HNF) flow over the vertical plate (VP), the set of dimensionless equations (27-29) is solved using the FORTRAN compiler. The compiler employs an implicit-based algorithm coupled with boundaries (30-32). The detailed numerical approximations are discussed by Doley et al. [46] Before obtaining the numerical solutions, the algorithm needs validation. Therefore, validation is performed against the published results by Muthucumaraswamy et al. [47].

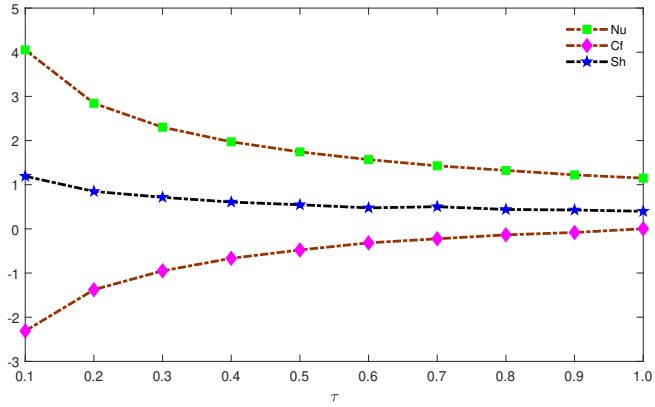

Fig. 2: Variation of Nu, Cf and Sh with respect to change in τ when $Gr = 5.0$, $Gc = 5.0$, $So = 0.1$, $Rn = 0.1$, $Du = 0.1$, $Q = 0.1$, $Q1 = 0.1$, $Ha = 2.5$, $Sc = 0.25$, $Ec = 0.1$, $\phi = 0.02$ and $Rd = 1$.

IV. Results and Discussion

The results in terms of Ω (velocity along the distance Y), θ (temperature variation along the distance Y) and Υ (concentration distribution along the distance Y) are depicted to examine the flow characteristics of Al_2O_3-Cu-water HNF. In addition, Nu (heat transfer rate), Cf (skin friction) and Sh (mass transfer rate) of various HNF's such as of Al_2O_3-Cu-water, Ag-Cu-water, MWCNT-Cu-water and TiO_2-Cu-water HNF are compared/illustrated for the different values of dimensionless parameters such as $Da = 0.25,\ 0.5,\ 0.75$ and 1.0; $Ec = 0.01,\ 0.1,\ 0.2$ and 0.3; $Sc = 2.5,\ 5.0,\ 7.5$ and 10.0; $Ha = 2.5,\ 5.0,\ 7.5$ and 10.0; $Du = 0.01,\ 0.1,\ 0.2$ and 0.3; $So = 0.01,\ 0.1,\ 0.2$ and 0.3; $Gr = 2.5,\ 5.0,\ 7.5$ and 10.0; $Gc = 2.5,\ 5.0,\ 7.5$ and 10.0; $Rd = 0.1,\ 1.0,\ 2.0$ and 3.0; $Rn = 0.01,\ 0.1,\ 0.2$ and 0.3; $Q = 0.01,\ 0.1,\ 0.2$ and 0.3; $Q1 = 0.01,\ 0.1,\ 0.2$ and 0.3; $\phi = 0.01,\ 0.02,\ 0.03$ and 0.04. The volume fraction of nanoparticles is written as $\phi = \sum \phi_i = \phi_1 + \phi_2$.

Initially, the variation of heat and mass transfer rate by Cu-Al_2O_3-water HNF over the vertical plate with respect to time is illustrated in Fig. 2. The time is varied from $\tau = 0.1$ to 1.0. It is noted that Nu reduces with the increment in the Cf. This signifies the improvement of convection effect with respect to time. Moreover, mass transfer due to conduction decreases with time. With this information, the change in heat and mass transfer rate along with the HNF's velocity, temperature and concentration distribution is deeply investigated by changing the other parameter values at a fixed time ($\tau = 1.0$).

The examination of Ω, θ, and Υ for various values of Da when $Gr = 5.0$, $Gc = 5.0$, $So = 0.1$, $Rn = 0.1$, $Du = 0.1$, $Q = 0.1$, $Q1 = 0.1$, $Ha = 2.5$, $Sc = 0.25$, $Ec = 0.1$, $\phi = 0.02$, and $Rd = 1$ is encapsulated in Fig. 3. Here, the figure shows a wide variation of Ω from the boundary to $Y \leq 3.75$. Initially, Ω rises until a maximal position and asymptotically reduces. The maximal point is higher for higher values of Da. This is due to the improvement of permeability along the space Y. An improvement in permeability leads the HNF to flow more actively than in the lower Da case. Approximately when $Y = 5.0$, the velocity reaches zero. On the other side, θ and Υ reduce asymptotically without rising more than the

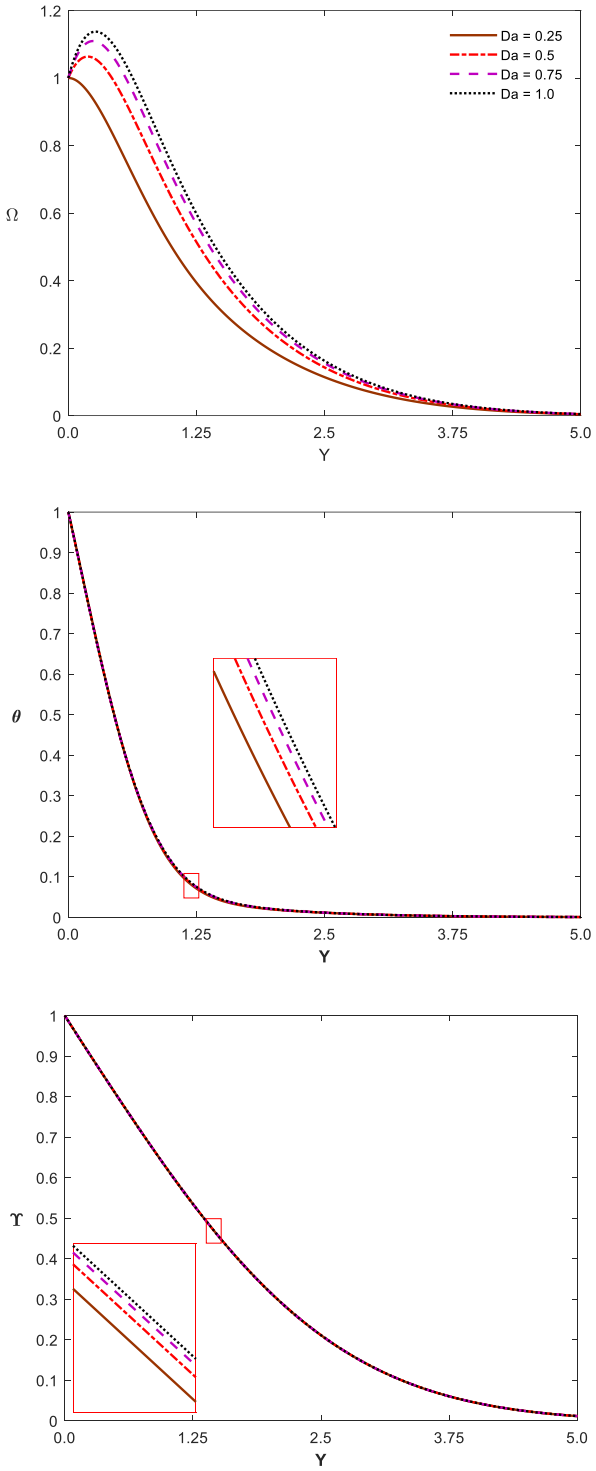

Fig. 3: Variation of Ω, θ and Υ with respect to Da when $Gr = 5.0$, $Gc = 5.0$, $So = 0.1$, $Rn = 0.1$, $Du = 0.1$, $Q = 0.1$, $Q1 = 0.1$, $Ha = 2.5$, $Sc = 0.25$, $Ec = 0.1$, $\phi = 0.02$ and $Rd = 1$.

boundary. It is noted that there is a small enhancement in the distribution of θ and Υ when increasing the permeability. However, more differences are found in the flow velocity.

Apart from the representation of Ω, θ, and Υ, the graphs for Nu, Cf, and Sh for various HNF are shown in Fig. 4. The results show an increase in Nu when increasing Da from 0.25 to 0.5. Furthermore, an increase in Da causes a

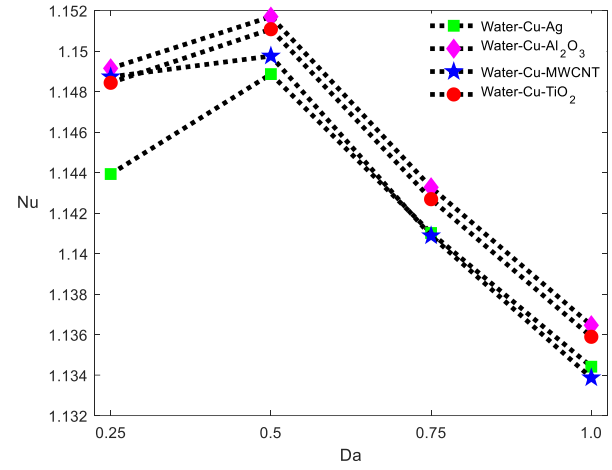

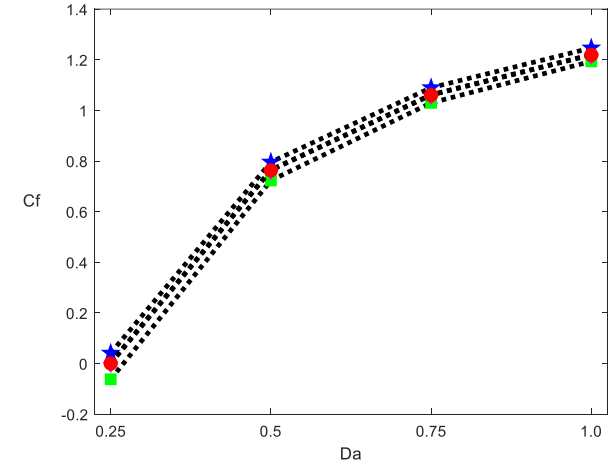

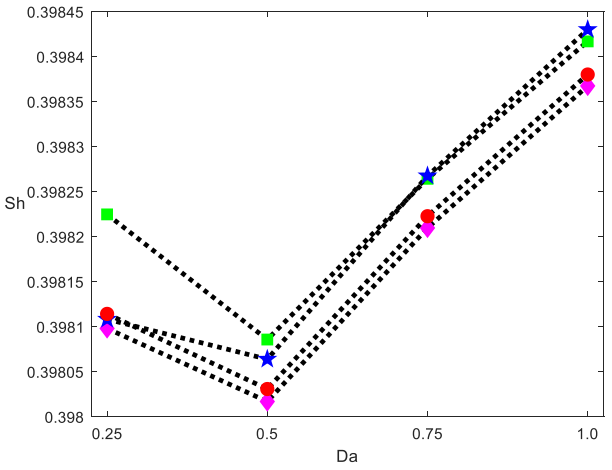

Fig. 4: Variation of Nu, Cf and Sh with respect to Da when $Gr = 5.0$, $Gc = 5.0$, $So = 0.1$, $Rn = 0.1$, $Du = 0.1$, $Q = 0.1$, $Q1 = 0.1$, $Ha = 2.5$, $Sc = 0.25$, $Ec = 0.1$, $\phi = 0.02$ and $Rd = 1$.

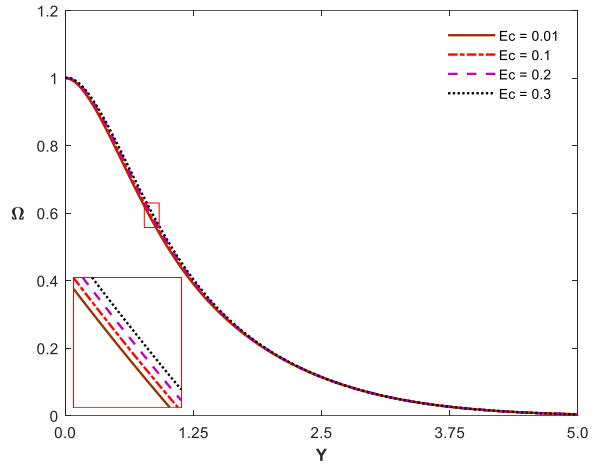

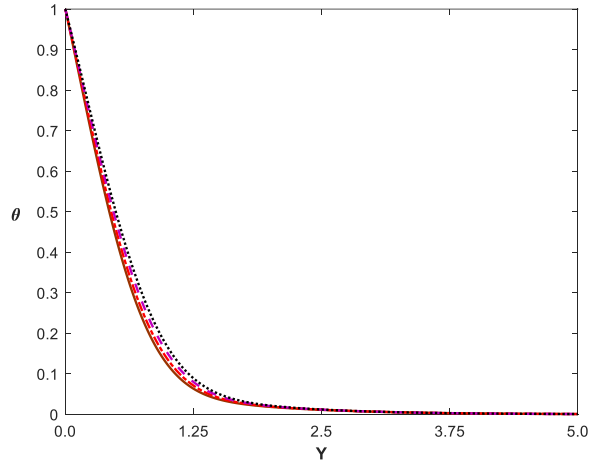

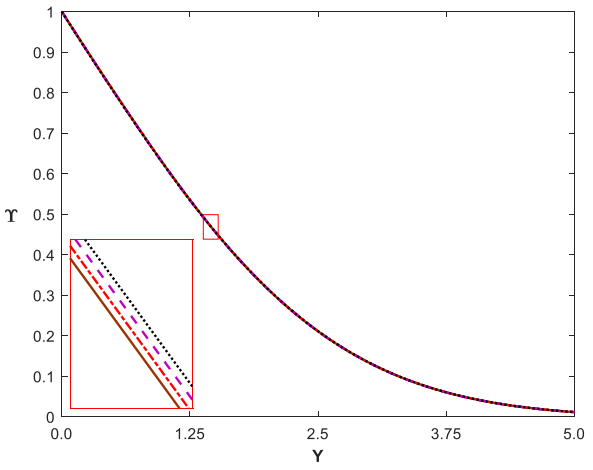

Fig. 5: Variation of Ω, θ and Υ with respect to Ec when $Gr = 5.0$, $Gc = 5.0$, $So = 0.1$, $Rn = 0.1$, $Du = 0.1$, $Q = 0.1$, $Q1 = 0.1$, $Ha = 2.5$, $Sc = 0.25$, $Da = 0.25$, $\phi = 0.02$ and $Rd = 1$.

depletion in Nu. On the other side, the opposite variation is spotted with Sh. Additionally, it is found that Cf increases for every increase in Da, denoting convection gain. The variation in Nu confirms the decrement of conduction and convection gain. The inverse plot is found with Sh, and the corresponding Cf plot represents the gain of convection mass transfer. Precisely, it is noted that the mass diffusivity reduces from $Da = 0.25$ to 0.5, and when $Da \geq 0.5$, convection mass transfer effect takes place. This shows the free flow of mass concerning an increase in permeability. The comparison of heat transport by various HNFs is made, and it is found that Al_2O_3-Cu-water HNF provides a higher heat transfer rate than the other HNFs. However, the Cf is higher for Cu-MWCNT-water HNF for every Da. Also, Cu-

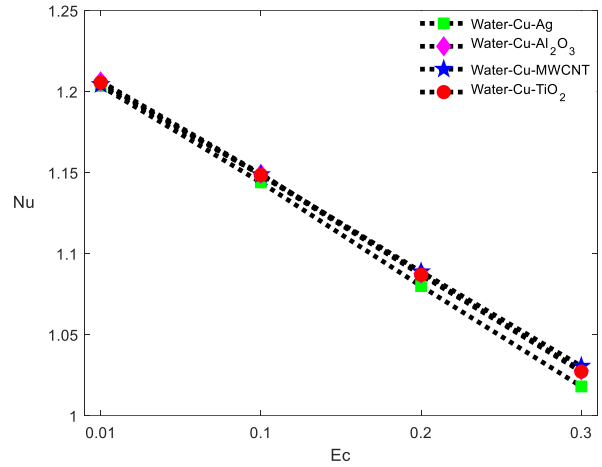

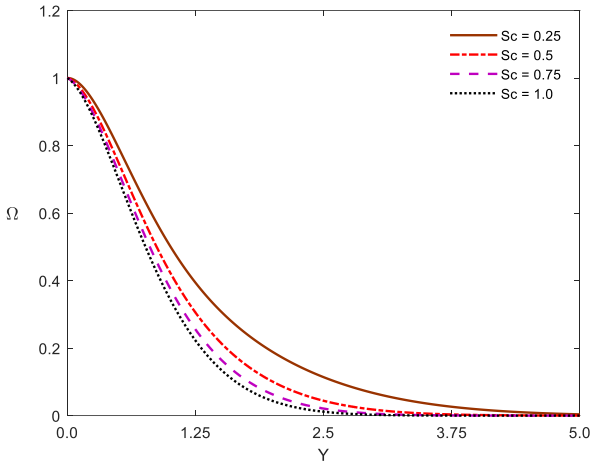

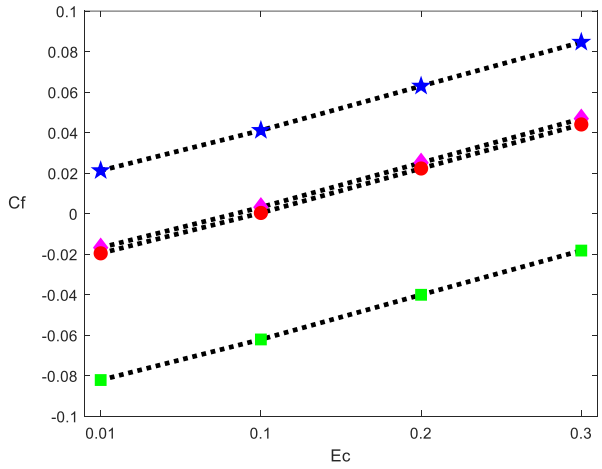

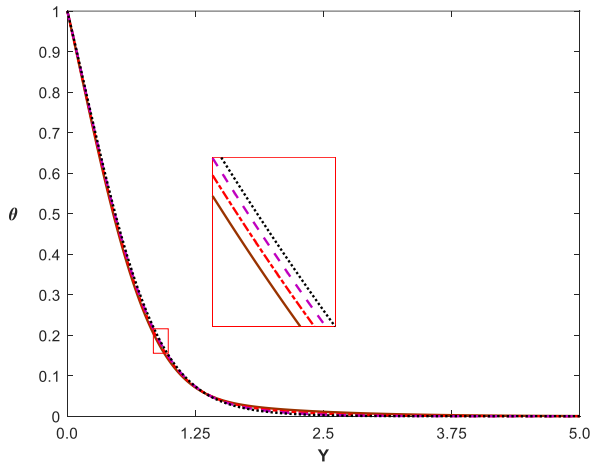

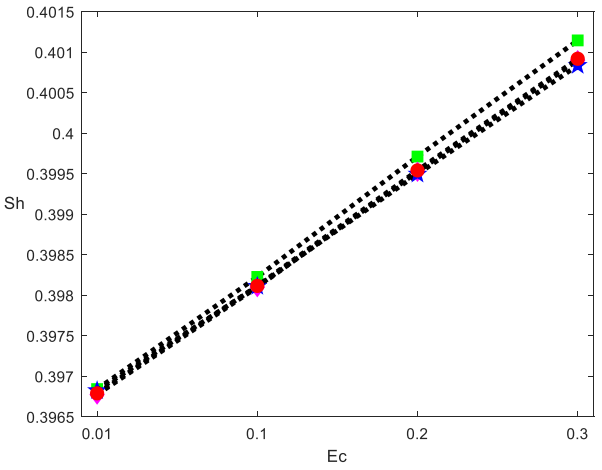

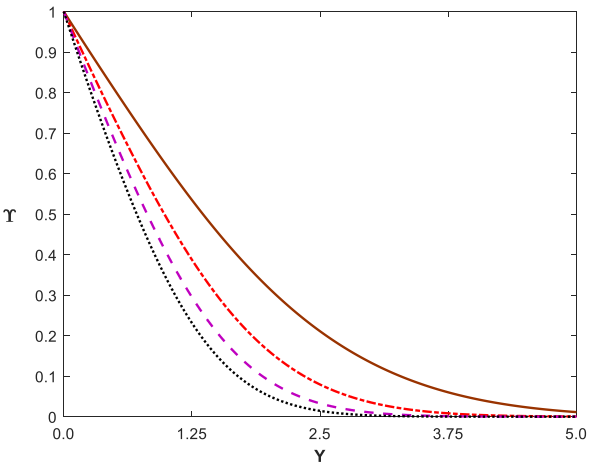

Fig. 6: Variation of Nu, Cf and Sh with respect to Ec when $Gr = 5.0$, $Gc = 5.0$, $So = 0.1$, $Rn = 0.1$, $Du = 0.1$, $Q = 0.1$, $Q1 = 0.1$, $Ha = 2.5$, $Sc = 0.25$, $Da = 0.25$, $\phi = 0.02$ and $Rd = 1$.

Fig. 7: Variation of Ω, θ and Υ with respect to Sc when $Gr = 5.0$, $Gc = 5.0$, $So = 0.1$, $Rn = 0.1$, $Du = 0.1$, $Q = 0.1$, $Q1 = 0.1$, $Ha = 2.5$, $Da = 0.25$, $Ec = 0.1$, $\phi = 0.02$ and $Rd = 1$.

MWCNT-water HNF delivers a higher Sh for higher Da.

The effects of viscous dissipation on fluid flow and heat transfer are illustrated in Figs. 5 and 6 when $Gr = 5.0$, $Gc = 5.0$, $So = 0.1$, $Rn = 0.1$, $Du = 0.1$, $Q = 0.1$, $Q1 = 0.1$, $Ha = 2.5$, $Sc = 0.25$, $Da = 0.25$, and $\phi = 0.02$. The Eckert number varied from 0.01 to 0.3. As Ec increases, the velocity (Ω) reduces from the boundary. This contrasts with the case of increasing Darcy number, which leads to a rise in Ω beyond the boundary. A small variation is noted with Ec compared to the significant effect of Darcy number. The Eckert number represents the advective transport of the nanofluid, bridging the HNF's flow kinetic energy and enthalpy boundary layer. Thus, viscous dissipation effects contribute to an increase in Ω. Additionally, due to the shear

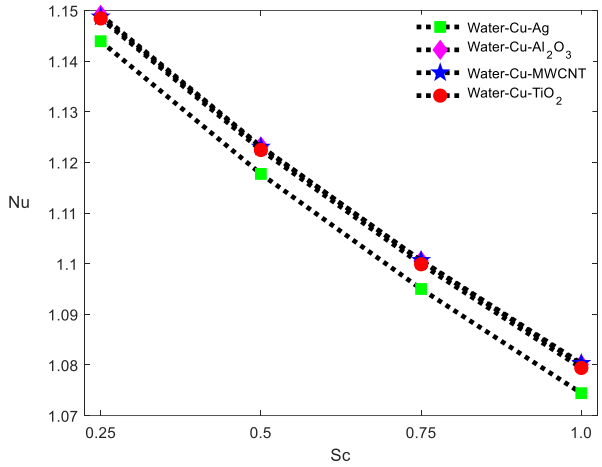

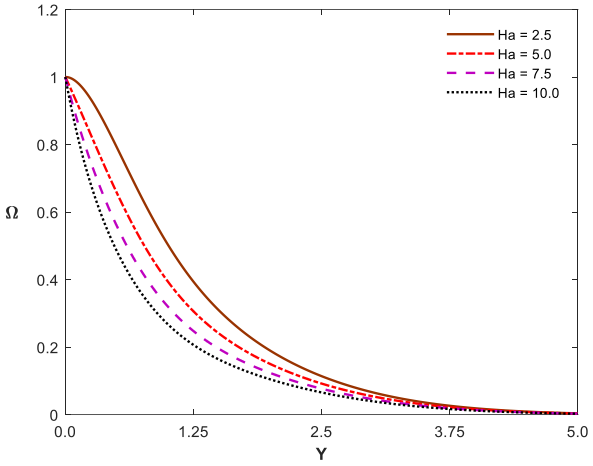

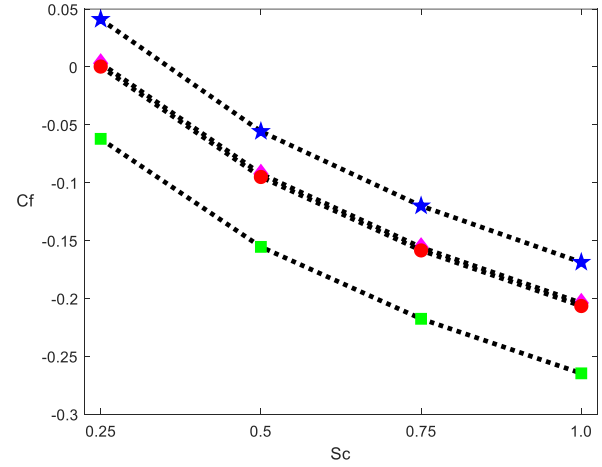

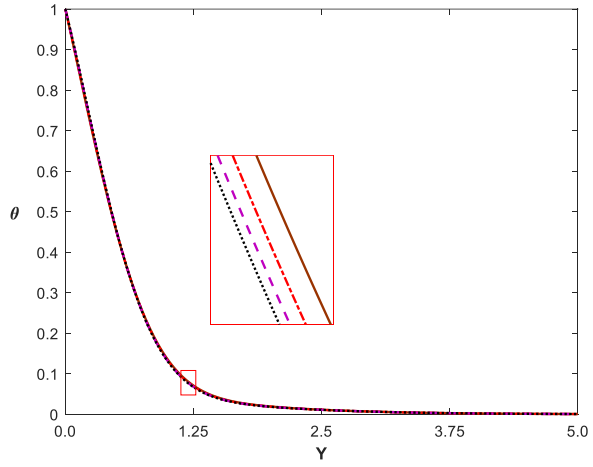

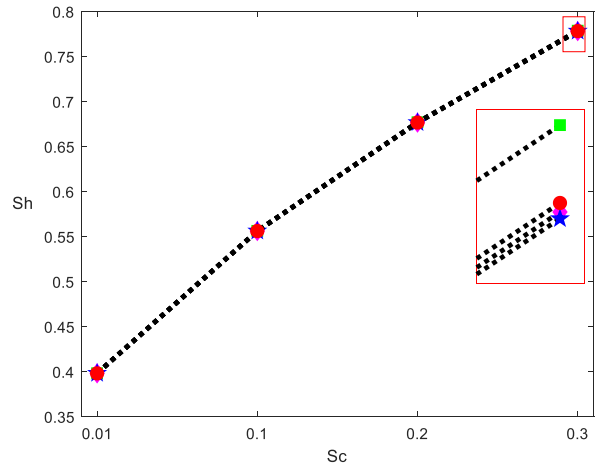

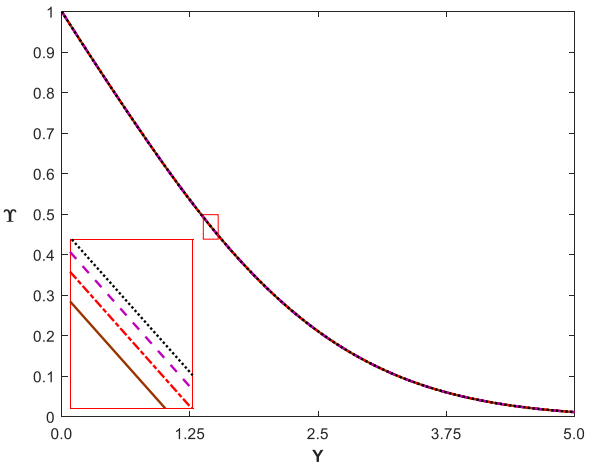

Fig. 8: Variation of Nu, Cf and Sh with respect to Sc when $Gr = 5.0$, $Gc = 5.0$, $So = 0.1$, $Rn = 0.1$, $Du = 0.1$, $Q = 0.1$, $Q1 = 0.1$, $Ha = 2.5$, $Da = 0.25$, $Ec = 0.1$, $\phi = 0.02$ and $Rd = 1$.

Fig. 9: Variation of Ω, θ and Υ with respect to Ha when $Gr = 5.0$, $Gc = 5.0$, $So = 0.1$, $Rn = 0.1$, $Du = 0.1$, $Q = 0.1$, $Q1 = 0.1$, $Da = 0.25$, $Sc = 0.25$, $Ec = 0.1$, $\phi = 0.02$ and $Rd = 1$.

force generated from HNF kinetic energy conversion to heat, an increase in θ is observed. A slight rise in Υ is also noticed with Ec. The comparison of various HNFs in terms of Nu, Cf, and Sh by varying Ec is shown in Fig. 5(b). The reduction of Nu and the increase in Cf are noted with the rise in Ec. The energy generated from fluid motion improves heat transfer, leading to an increase in Cf and convection heat transfer. However, the Nu plot shows a decrease in conduction heat transfer rate. The thermophysical properties of MWCNT nanoparticles make Cu-MWCNT-water HNF exhibit higher Nu and Cf with respect to viscous dissipation effects. Also, Cu-Ag-water HNF exhibits lower Nu and Cf. In contrast to Nu, the Sherwood number increases with Ec. As Cf increases, mass transfer is stimulated through

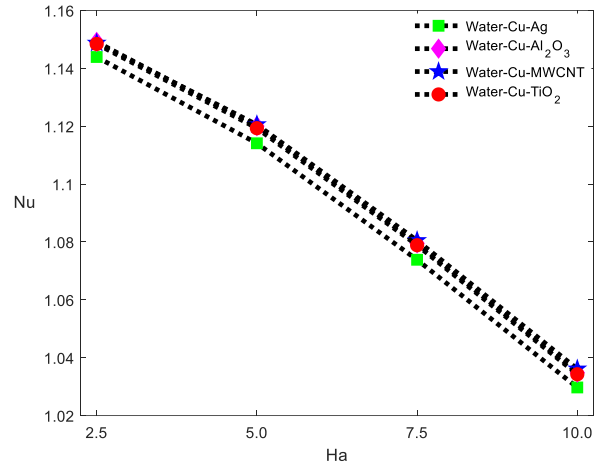

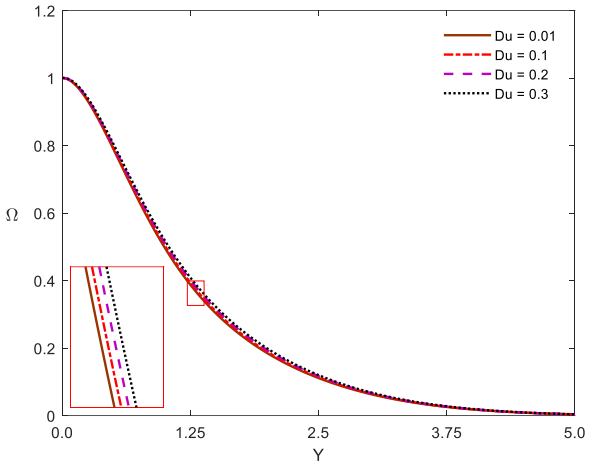

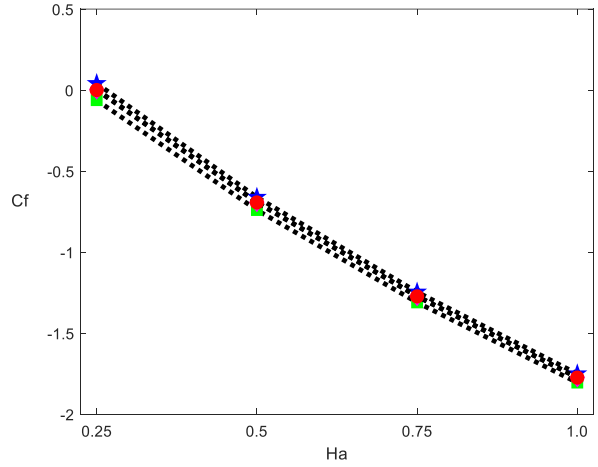

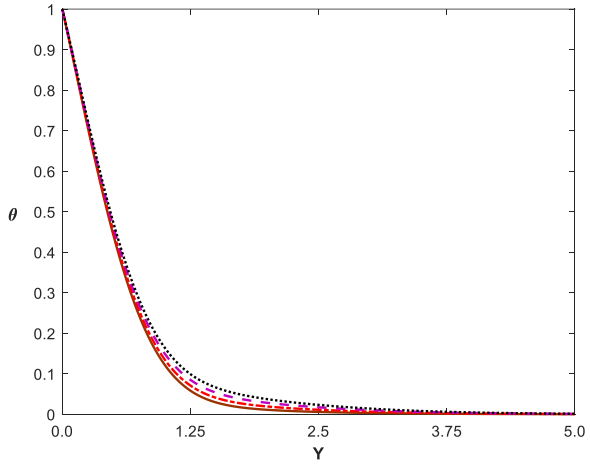

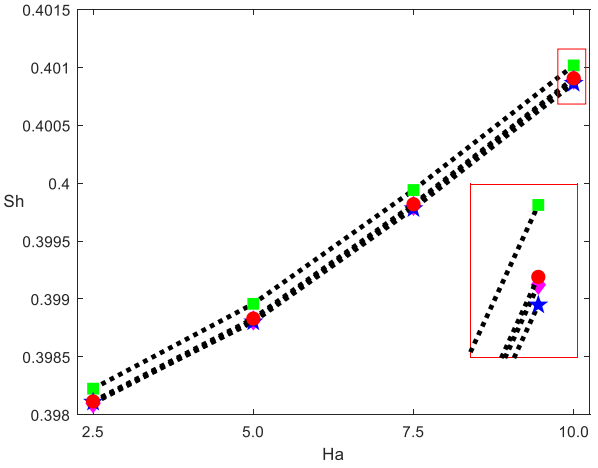

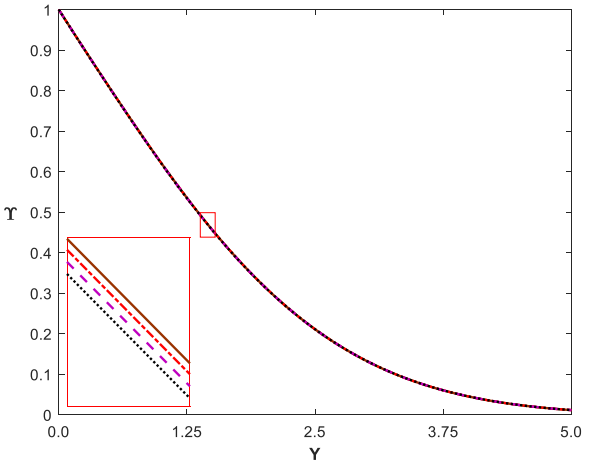

Fig. 10: Variation of Nu, Cf and Sh with respect to Ha when $Gr = 5.0$, $Gc = 5.0$, $So = 0.1$, $Rn = 0.1$, $Du = 0.1$, $Q = 0.1$, $Q1 = 0.1$, $Da = 0.25$, $Sc = 0.25$, $Ec = 0.1$, $\phi = 0.02$ and $Rd = 1$.

Fig. 11: Variation of Ω, θ and Υ with respect to Du when $Gr = 5.0$, $Gc = 5.0$, $So = 0.1$, $Rn = 0.1$, $Da = 0.25$, $Q = 0.1$, $Q1 = 0.1$, $Ha = 2.5$, $Sc = 0.25$, $Ec = 0.1$, $\phi = 0.02$ and $Rd = 1$.

convection. In the case of mass transport, Cu-Ag-water HNF provides a higher Sh, while Cu-MWCNT-water HNF provides a lower Sh.

The variation of Ω, θ, and Υ along the Y direction with respect to different Sh values is illustrated in Fig. 7, while the plots representing Nu, Cf, and Sh are depicted in Fig. 8. The plots for Ω, θ, and Υ are generated under the conditions $Gr = 5.0$, $Gc = 5.0$, $So = 0.1$, $Rn = 0.1$, $Du = 0.1$, $Q = 0.1$, $Q1 = 0.1$, $Ha = 2.5$, $Da = 0.25$, $Ec = 0.1$, $\phi = 0.02$, and $Rd = 1$. The Schmid number is increased to 0.25, 0.5, 0.75, and 1.0. The increment in Sc results in a reduction in Ω in the Y direction. The flow asymptotically decreases to zero, and the increment in Sc leads to achieving zero velocity at a shorter Y distance. This reduction

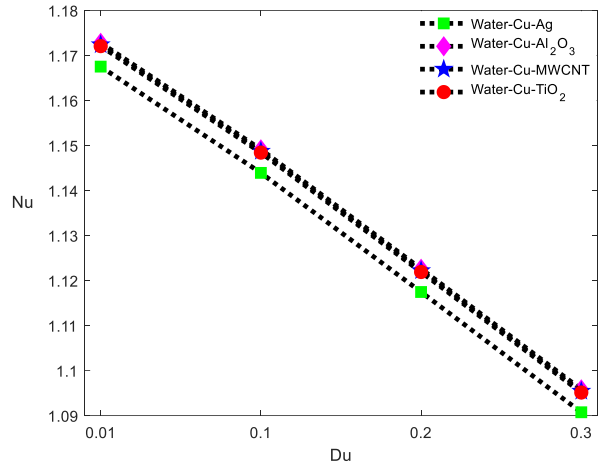

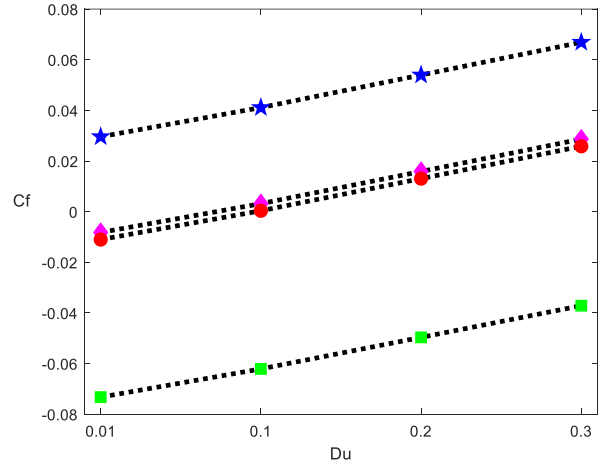

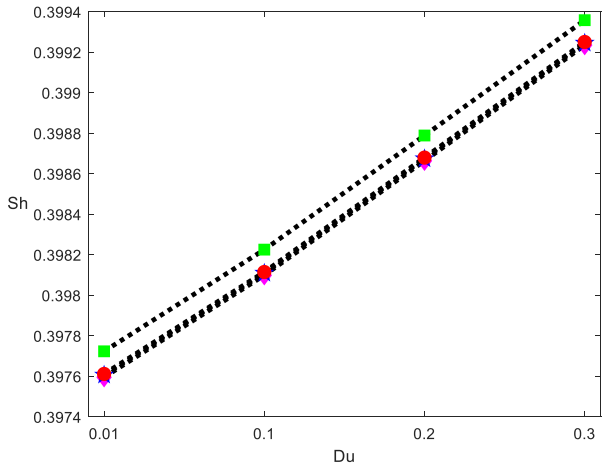

Fig. 12: Variation of Nu, Cf and Sh with respect to Du when $Gr = 5.0$, $Gc = 5.0$, $So = 0.1$, $Rn = 0.1$, $Da = 0.25$, $Q = 0.1$, $Q1 = 0.1$, $Ha = 2.5$, $Sc = 0.25$, $Ec = 0.1$, $\phi = 0.02$ and $Rd = 1$.

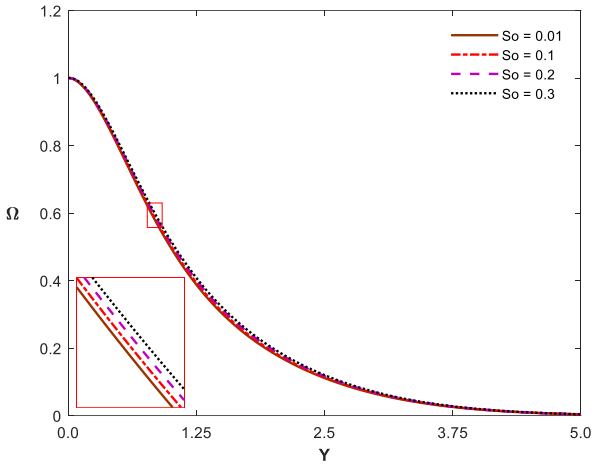

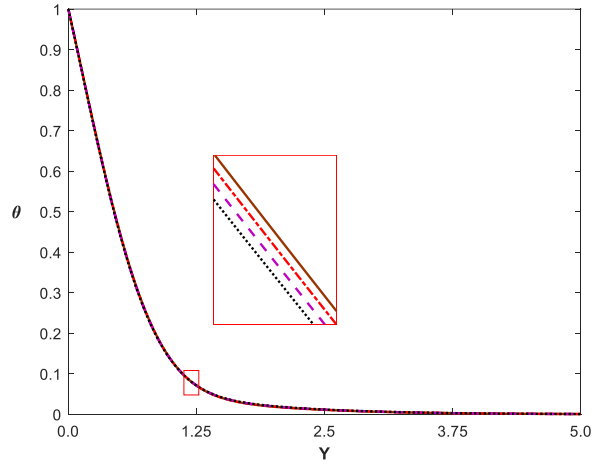

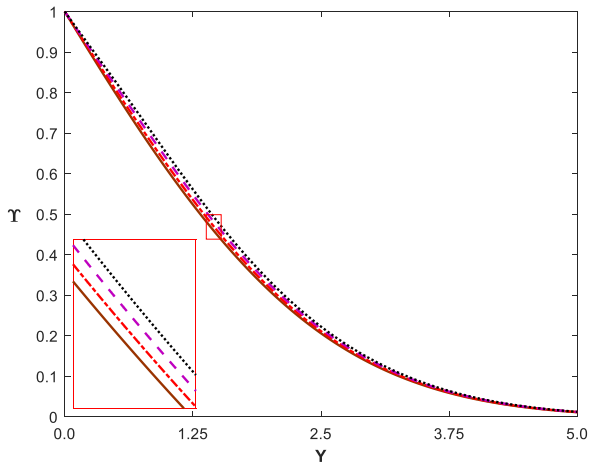

Fig. 13: Variation of Ω, θ and Υ with respect to So when $Gr = 5.0$, $Gc = 5.0$, $Da = 0.25$, $Rn = 0.1$, $Du = 0.1$, $Q = 0.1$, $Q1 = 0.1$, $Ha = 2.5$, $Sc = 0.25$, $Ec = 0.1$, $\phi = 0.02$ and $Rd = 1$.

in Ω is attributed to the decrease in molecular diffusion, causing a reduction in heat transfer as well. Furthermore, it is observed that the Nusselt number of Cu-Al_2O_3-water HNF is higher than that of other HNFs, while Cu-Ag-water HNF provides a lower Nu. Similar to Nu, skin friction (Cf) decreases with increasing Sh, and Cu-Al_2O_3-water HNF exhibits higher Cf. Following Cu-Al_2O_3-water HNF, Cu-MWCNT-water HNF, and Cu-TiO_2-water HNF provide higher heat transfer rates. The elevated Nu of HNFs is attributed to the unique thermophysical properties of each nanoparticle. By comparing Nu and Cf plots, it is evident that convection-based heat transfer decreases with increasing Sh. Additionally, the temperature distribution shows a slight enhancement with Sh up to a distance of $Y = 1.25$, and a

marginal increment in θ is noted. The decrease in the effect of molecular diffusion significantly contributes to the reduction in Υ distribution. The concentration rapidly reaches zero with higher Sh, indicating an increase in conduction-based mass transfer.

Figures 9 and 10 illustrate the flow distribution and heat/mass transfer rates while varying the effects of an applied magnetic field under the conditions $Gr = 5.0$, $Gc = 5.0$, $So = 0.1$, $Rn = 0.1$, $Du = 0.1$, $Q = 0.1$, $Q1 = 0.1$, $Da = 0.25$, $Sc = 0.25$, $Ec = 0.1$, $\phi = 0.02$, and $Rd = 1$. It is observed that Ω decreases with the increase in Ha, and a minor reduction is also noticed with temperature distribution. The primary reason for the reduction in Ω and θ is the creation of a resistive nature associated with the Lorentz force. However, a small increment in concentration along the Y direction occurs due to the thickening or damping of flow and the corresponding concentration boundary layer. The Nu plot indicates a reduction in the heat transfer rate due to a decrease in convection or Ω. Initially, at $Ha = 2.5$, Cu-Al_2O_3-water HNF provides a higher Nu, followed by MWCNT, TiO_2, and Ag-based Cu-water HNFs. However, when we increase the effect of magnetic field (to $Ha = 5.0$ and 7.5), Cu-Al_2O_3-water HNF gradually reduces compared to Cu-MWCNT-water HNF. At $Ha = 10.0$, it is noted that the heat transfer rate of Cu-Al_2O_3-water HNF is lower than that of Cu-MWCNT-water and Cu-TiO_2-water HNFs. On the other hand, Cu-MWCNT-water HNF exhibits higher Cf and Sh. Additionally, due to damping effects, skin friction also reduces with Ha, indicating a decline in convection. This signals a decrease in convective mass transport with an increase in diffusive mass transport.

The role of the diffusion-thermo effect on HNF fluid flow over a vertical plate is illustrated by the variation in Du. An increase in Du influences HMT and fluid flow, as depicted in Figs. 11 and 12. The plots are visualized when $Gr = 5.0$, $Gc = 5.0$, $So = 0.1$, $Rn = 0.1$, $Da = 0.25$, $Q = 0.1$, $Q1 = 0.1$, $Ha = 2.5$, $Sc = 0.25$, $Ec = 0.1$, $\phi = 0.02$, and $Rd = 1$. The variation in Du has a minor impact on Ω, and an increase in Du results in a smaller increment in Ω. Moreover, the distribution of θ increases along the distance Y with the increase in Du. The rise in Ω is due to the increase in the distribution of θ, which is caused by the mass concentration gradient on temperature effects. Also, concerning Du, the thickness of the concentration layer decreases, resulting in a smaller fall in Υ. Overall, Cf increases with Du due to the rise in natural convection effect, and a decrease in Nu is observed with increasing Du. The conduction-based heat transfer decreases due to the upshot in convection. As in the previous plot, heat transfer by various HNF follows the order Cu-Al_2O_3-water, Cu-MWCNT-water, Cu-TiO_2-water, and Cu-Ag-water, respectively. The mass transfer order by various HNFs is just the reverse order of Nu. However, in the case of Cf, Cu-MWCNT-water NHF provides a higher skin friction rate, followed by Cu-Al_2O_3-water, Cu-TiO_2-water, and Cu-Ag-water HNF.

Similar to the diffusion-thermo behavior, the role of thermal diffusion in HMT fluid flow when $Gr = 5.0$, $Gc = 5.0$, $Da = 0.25$, $Rn = 0.1$, $Du = 0.1$, $Q = 0.1$, $Q1 = 0.1$, $Ha = 2.5$, $Sc = 0.25$, $Ec = 0.1$, $\phi = 0.02$, and $Rd = 1$ is depicted in Figs. 13 and 14. The concentration is distributed under the influence of the thermal gradient, causing an

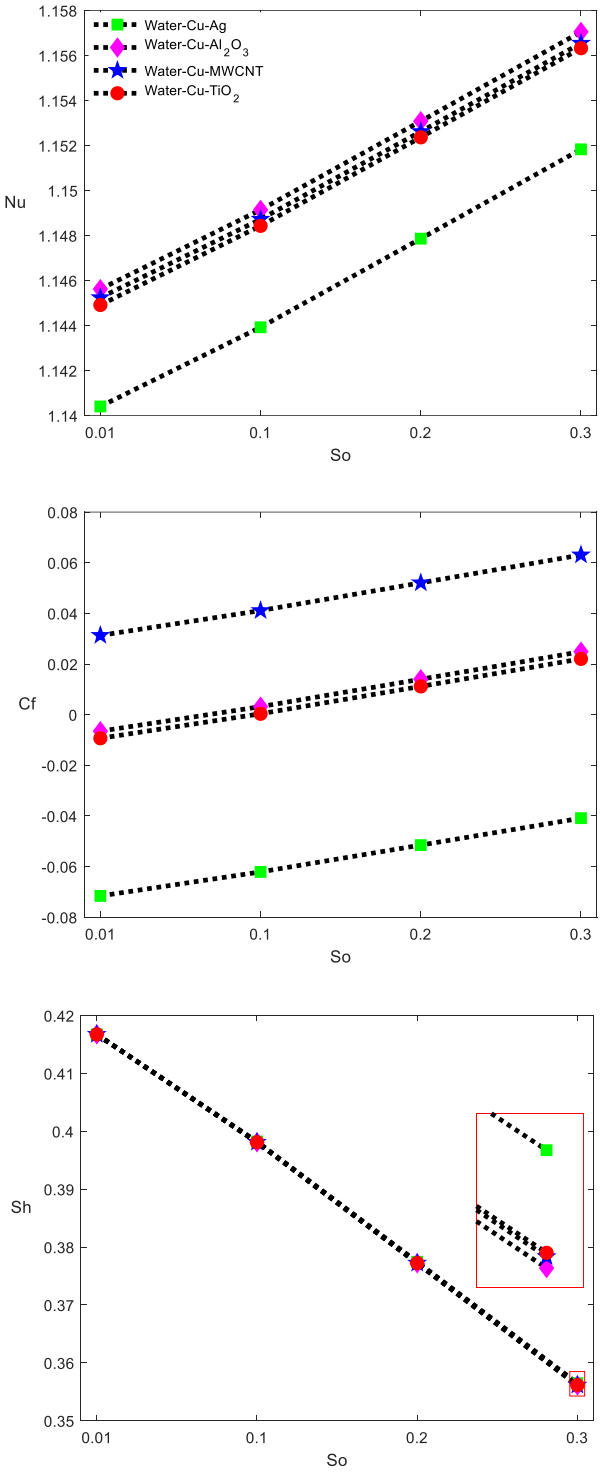

Fig. 14: Variation of Nu, Cf and Sh with respect to So when $Gr = 5.0$, $Gc = 5.0$, $Da = 0.25$, $Rn = 0.1$, $Du = 0.1$, $Q = 0.1$, $Q1 = 0.1$, $Ha = 2.5$, $Sc = 0.25$, $Ec = 0.1$, $\phi = 0.02$ and $Rd = 1$.

increase in Υ distribution and thus enhancing Ω. The rise in Υ is mainly due to the temperature gradient or the respective thermal boundary layer. In contrast to Du, the Soret number makes a smaller reduction in θ. Since So is the ratio of the difference in θ to Υ. Furthermore, it is noted that both the Nu and Cf plots rise with the increment in So. Thus, the heat transfer associated with the flow is due to convection.

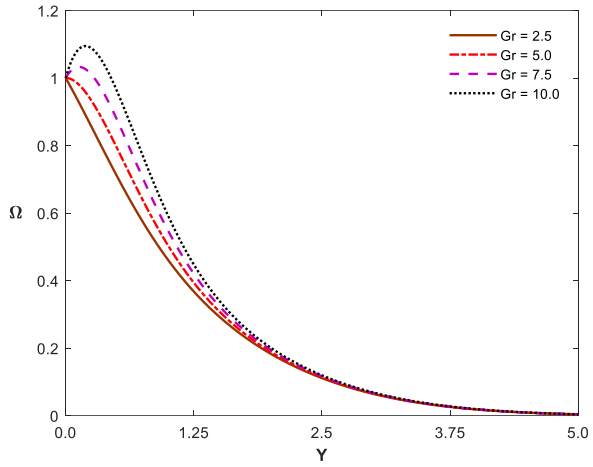

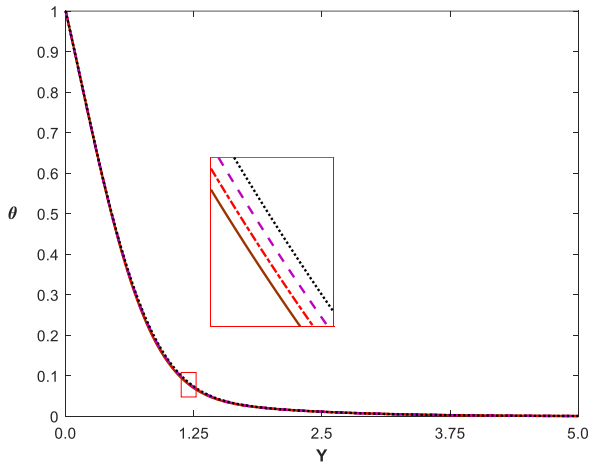

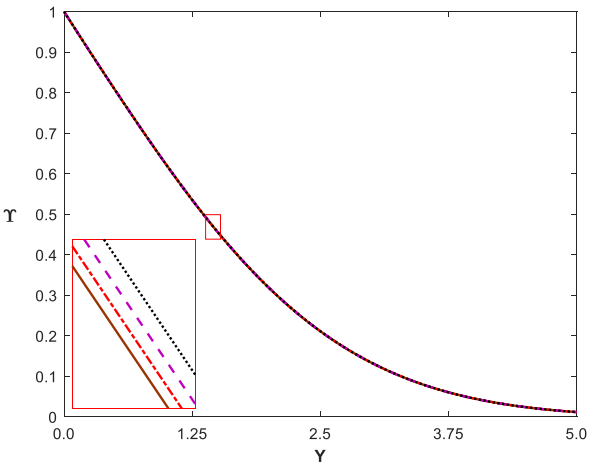

Fig. 15: Variation of Ω, θ and Υ with respect to Gr when $Da = 0.25$, $Gc = 5.0$, $So = 0.1$, $Rn = 0.1$, $Du = 0.1$, $Q = 0.1$, $Q1 = 0.1$, $Ha = 2.5$, $Sc = 0.25$, $Ec = 0.1$, $\phi = 0.02$ and $Rd = 1$.

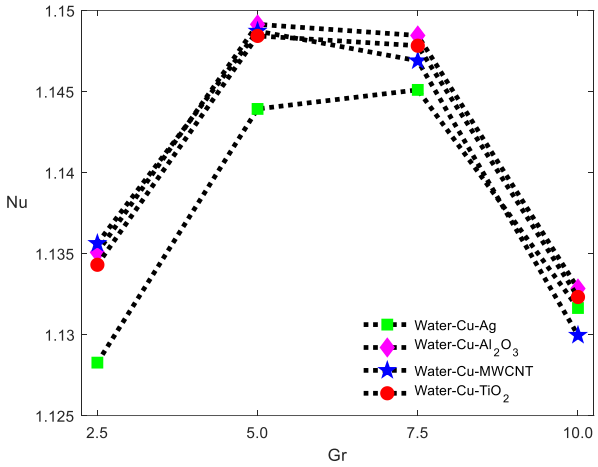

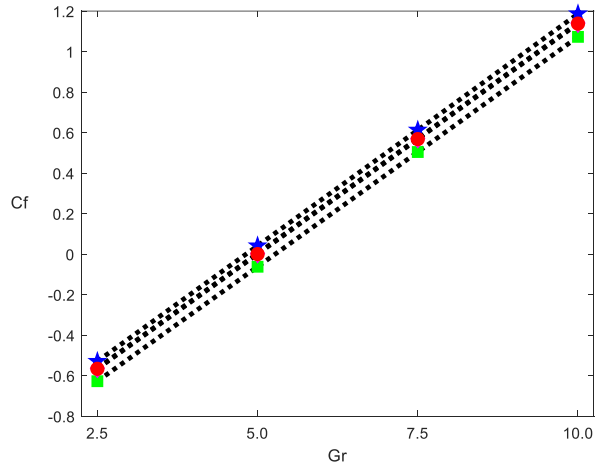

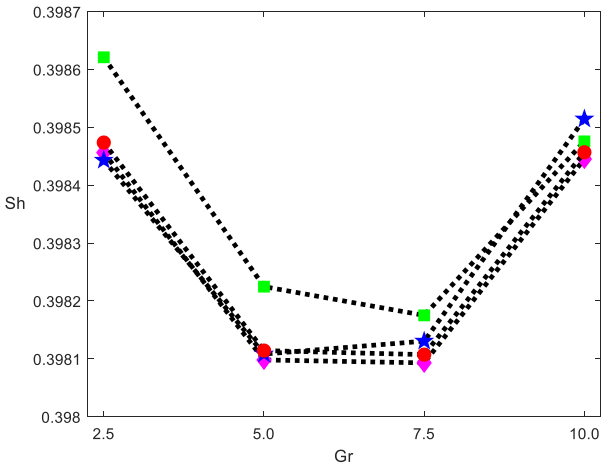

Fig. 16: Variation of Nu, Cf and Sh with respect to Gr when $Da = 0.25$, $Gc = 5.0$, $So = 0.1$, $Rn = 0.1$, $Du = 0.1$, $Q = 0.1$, $Q1 = 0.1$, $Ha = 2.5$, $Sc = 0.25$, $Ec = 0.1$, $\phi = 0.02$ and $Rd = 1$.

Similar to the Dufort effect, Cu-Al_2O_3-water NHF provides better heat transfer. However, the difference in heat transfer between Cu-Al_2O_3-water and Cu-MWCNT-water HNF is more pronounced in the case of the Soret effect. The Sh plots, on the other hand, reduce with So in contrast to Nu and Cf. This illustrates the reduction of mass diffusivity with the Soret number. Also, Cu-Ag-water HNF provides a higher Sh and Cu-Al_2O_3-water HNF provides a lower Sh.

Natural convection effects play a vital role in fluid flow phenomena, and the respective variations in Ω, θ, and Υ plots are noted by varying Gr. The plots are depicted in Fig. 15 when $Da = 0.25$, $Gc = 5.0$, $So = 0.1$, $Rn = 0.1$, $Du = 0.1$, $Q = 0.1$, $Q1 = 0.1$, $Ha = 2.5$, $Sc = 0.25$, $Ec = 0.1$, $\phi = 0.02$, and $Rd = 1$. At $Gr = 2.5$, the plot of Ω

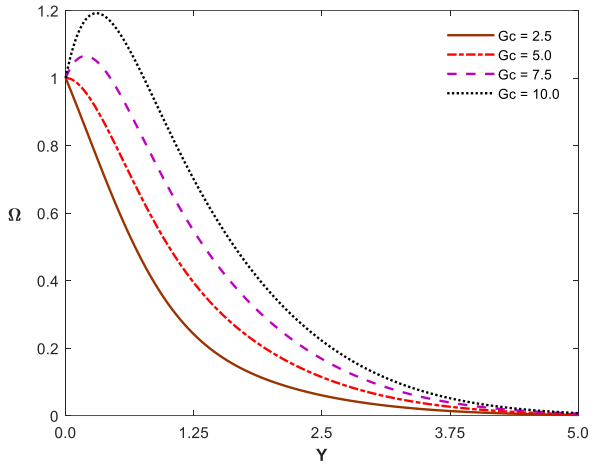

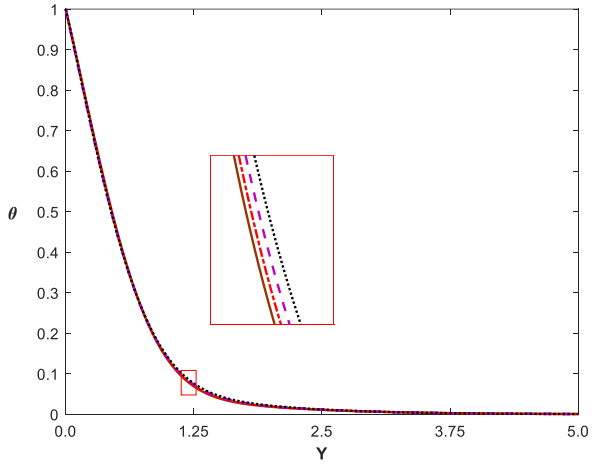

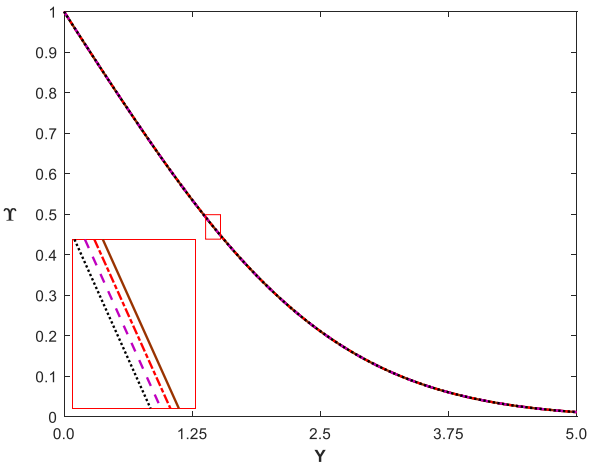

Fig. 17: Variation of Ω, θ and Υ with respect to Gc when $Gr = 5.0$, $Da = 0.25$, $So = 0.1$, $Rn = 0.1$, $Du = 0.1$, $Q = 0.1$, $Q1 = 0.1$, $Ha = 2.5$, $Sc = 0.25$, $Ec = 0.1$, $\phi = 0.02$ and $Rd = 1$.

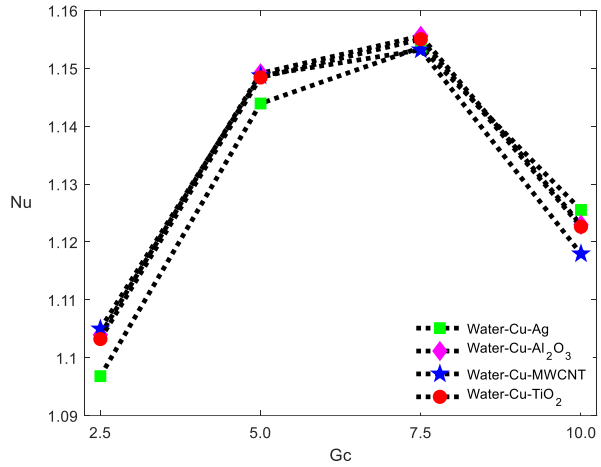

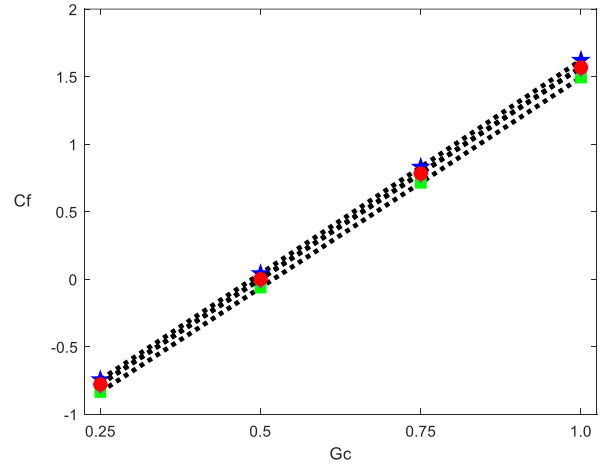

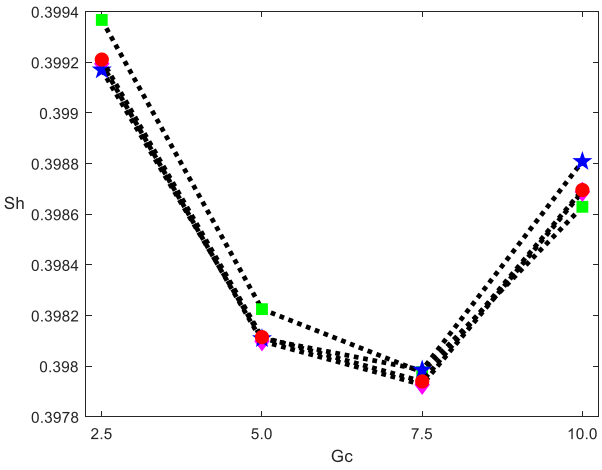

Fig. 18: Variation of Nu, Cf and Sh with respect to Gc when $Gr = 5.0$, $Da = 0.25$, $So = 0.1$, $Rn = 0.1$, $Du = 0.1$, $Q = 0.1$, $Q1 = 0.1$, $Ha = 2.5$, $Sc = 0.25$, $Ec = 0.1$, $\phi = 0.02$ and $Rd = 1$.

reduces asymptotically to zero. With an increase in Gr to 5.0, the velocity rises slightly from the boundary and then falls to zero. Further increases above $Gr = 5.0$ result in Ω rising above the boundary due to the density variation developed with the increase in convection effects. Here, Ω rises and attains peak velocity at a certain distance and subsequently reduces to zero velocity. This peak velocity and its position change with various values of Gr. However, the HNF reaches zero velocity (approximately) at the same distance ($Y = 5.0$) with various values of Gr. Apart from Ω, the temperature and concentration show lesser variation with Gr. A small increase is noted in θ and Υ. The HMT associated with the flow is shown in Fig. 16. It is observed that Nu increases up to a certain value of Gr and then decreases. However,

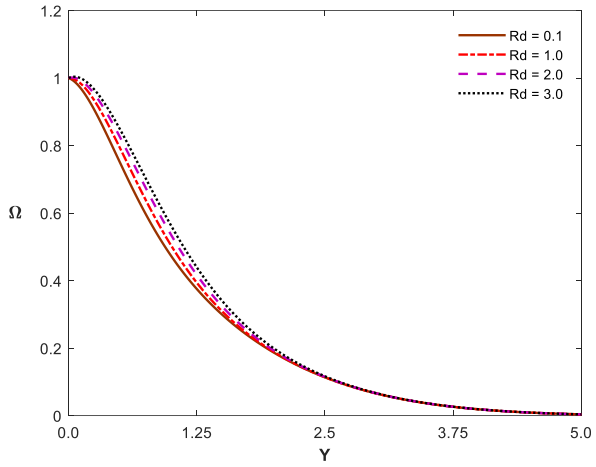

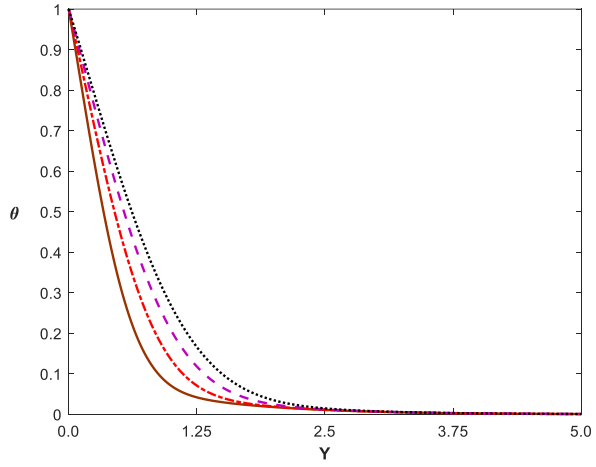

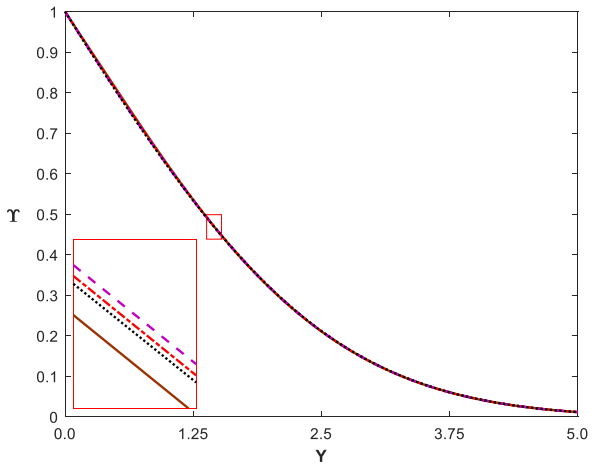

Fig. 19: Variation of Ω, θ and Υ with respect to Rd when $Gr = 5.0$, $Da = 0.25$, $So = 0.1$, $Rn = 0.1$, $Du = 0.1$, $Q = 0.1$, $Q1 = 0.1$, $Ha = 2.5$, $Sc = 0.25$, $Ec = 0.1$, $\phi = 0.02$ and $Da = 0.25$.

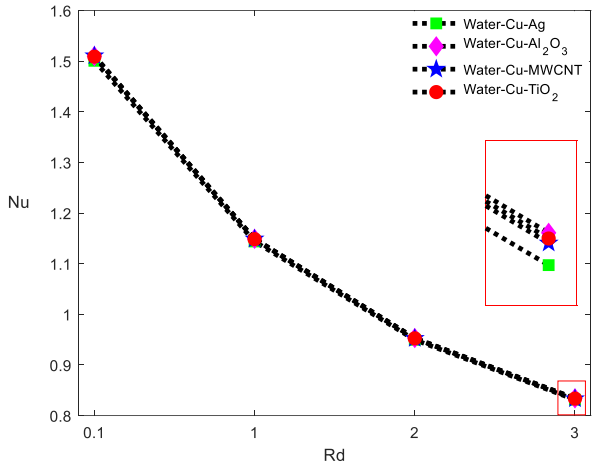

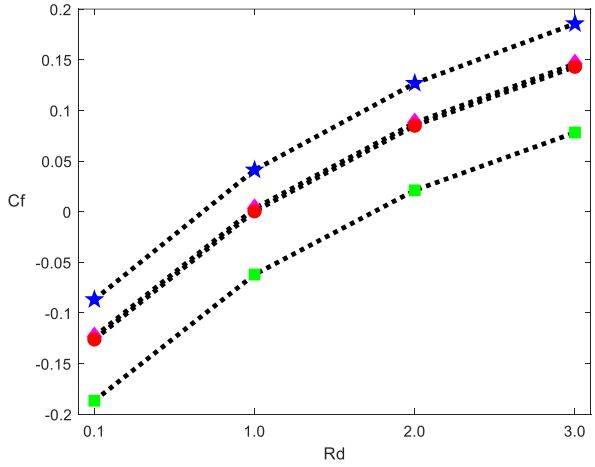

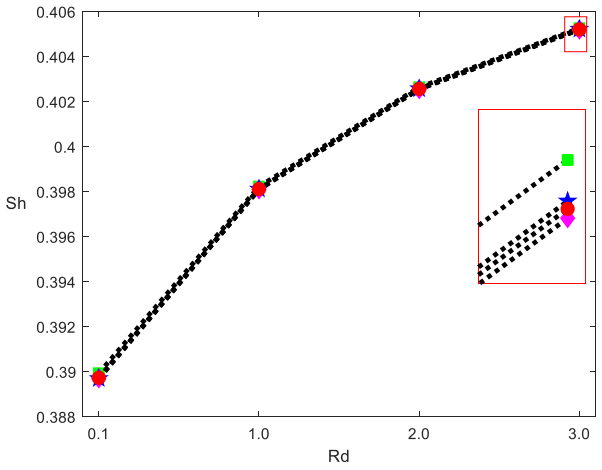

Fig. 20: Variation of Nu, Cf and Sh with respect to Rd when $Gr = 5.0$, $Da = 0.25$, $So = 0.1$, $Rn = 0.1$, $Du = 0.1$, $Q = 0.1$, $Q1 = 0.1$, $Ha = 2.5$, $Sc = 0.25$, $Ec = 0.1$, $\phi = 0.02$ and $Da = 0.25$.

there is only improvement in Cf is noticed, illustrating the growth of convection. Also, the decrease in Nu when $Gr \geq 5.0$ shows the development of buoyancy force. The reverse reaction happens in the Sh plots. Sh increases when $Gr \geq 5.0$ due to convection mass transfer. Also, when Gr is smaller ($Gr = 2.5$), Cu-MWCNT-water HNF provides higher Nu, followed by Cu-Al_2O_3-water and Cu-TiO_2-water HNFs. However, when $Gr = 10.0$, Cu-Al_2O_3-water provides higher heat transfer, followed by Cu-TiO_2-water and Cu-Ag-water HNFs. This scenario is due to heat transfer dependency. In the case of lower Gr, heat transfer is mainly due to conduction, and when Gr is larger, heat transfer is mainly due to convection.

The effect of the mass Grashof number on flow variables

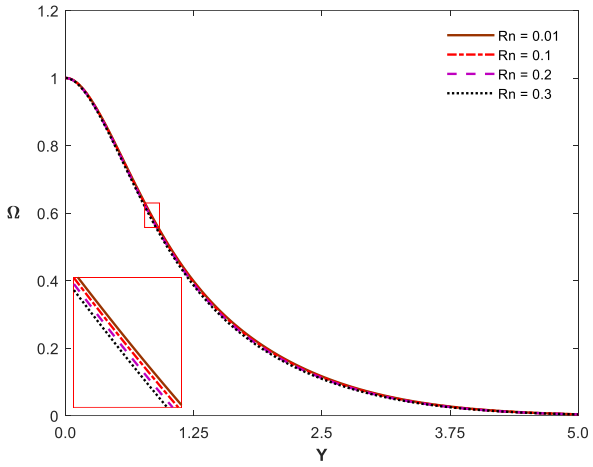

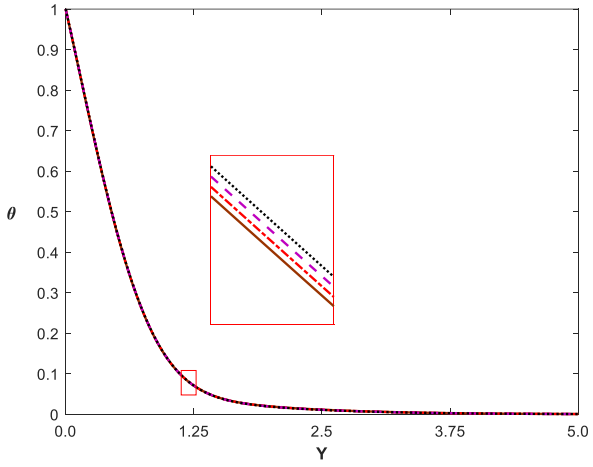

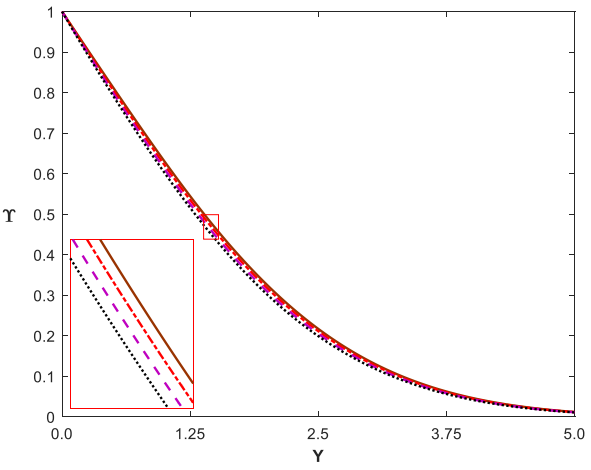

Fig. 21: Variation of Ω, θ and Υ with respect to Rn when $Gr = 5.0$, $Gc = 5.0$, $So = 0.1$, $Da = 0.25$, $Du = 0.1$, $Q = 0.1$, $Q1 = 0.1$, $Ha = 2.5$, $Sc = 0.25$, $Ec = 0.1$, $\phi = 0.02$ and $Rd = 1$.

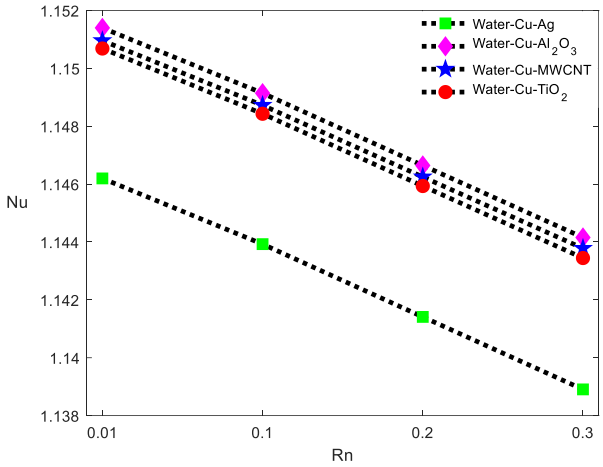

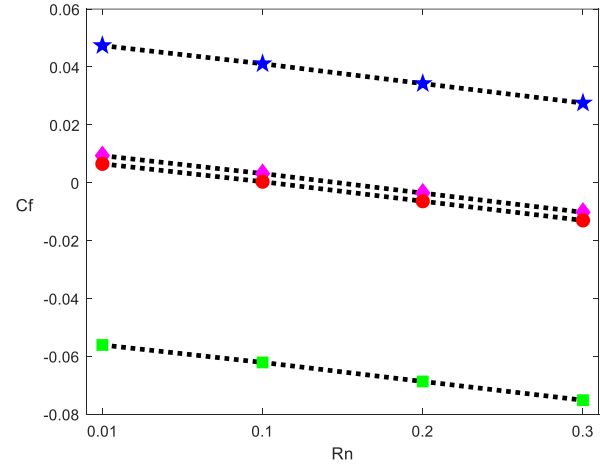

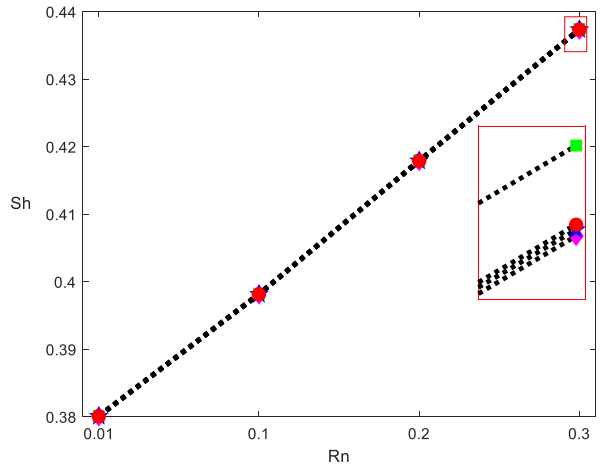

Fig. 22: Variation of Nu, Cf and Sh with respect to Rn when $Gr = 5.0$, $Gc = 5.0$, $So = 0.1$, $Da = 0.25$, $Du = 0.1$, $Q = 0.1$, $Q1 = 0.1$, $Ha = 2.5$, $Sc = 0.25$, $Ec = 0.1$, $\phi = 0.02$ and $Rd = 1$.

and HMT is depicted in Figs. 17 and 18 when $Gr = 5.0$, $Da = 0.25$, $So = 0.1$, $Rn = 0.1$, $Du = 0.1$, $Q = 0.1$, $Q1 = 0.1$, $Ha = 2.5$, $Sc = 0.25$, $Ec = 0.1$, $\phi = 0.02$, and $Rd = 1$. The Ω plot shows a significant variation with the enhancement of Gc compared to the enhancement of Gr. This is associated with the distribution of concentration and temperature. As seen in the figure, θ reaches zero near the distance $Y = 3.0$, and Υ reaches zero away from the distance $Y = 5.0$. Additionally, for the specified values of the above non-dimensional variables, the distribution of concentration is higher. In the case of advancing Gc, Ω improves significantly, while θ improves to a lesser extent. A small reduction in Υ occurs. However, only enhancement in all Ω, θ, and Υ occurs with the increment in Gr. The variation of

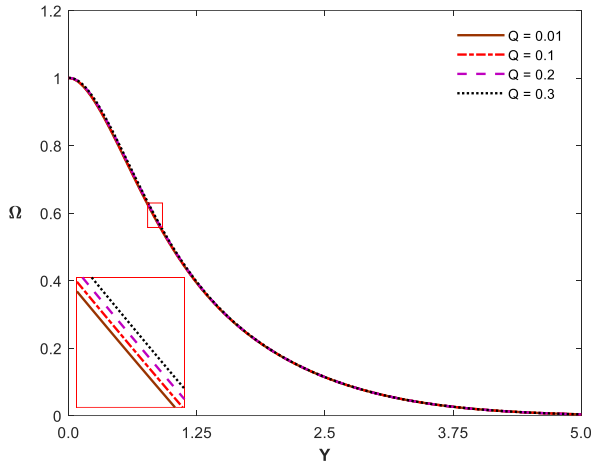

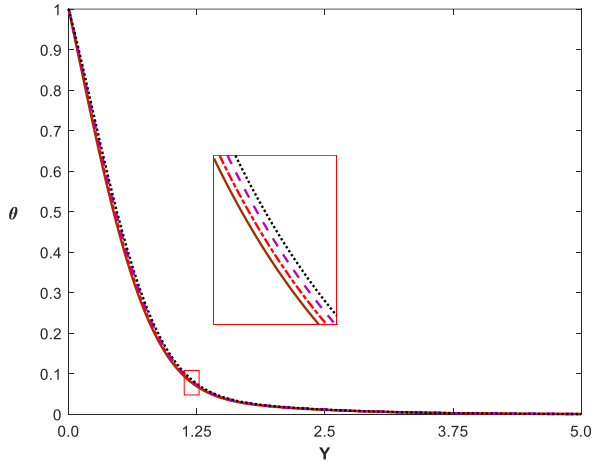

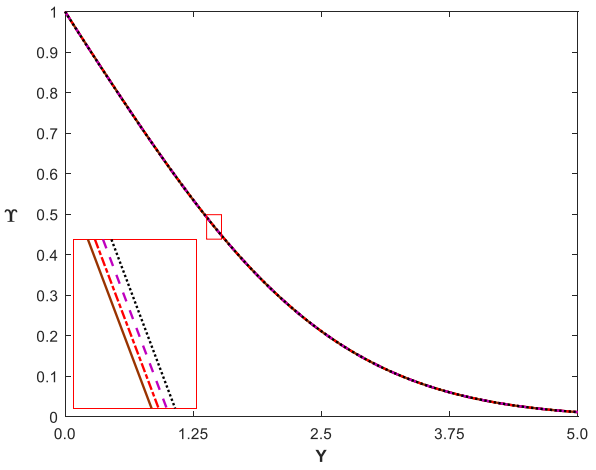

Fig. 23: Variation of Ω, θ and Υ with respect to Q when $Gr = 5.0$, $Gc = 5.0$, $So = 0.1$, $Rn = 0.1$, $Du = 0.1$, $Da = 0.25$, $Q1 = 0.1$, $Ha = 2.5$, $Sc = 0.25$, $Ec = 0.1$, $\phi = 0.02$ and $Rd = 1$.

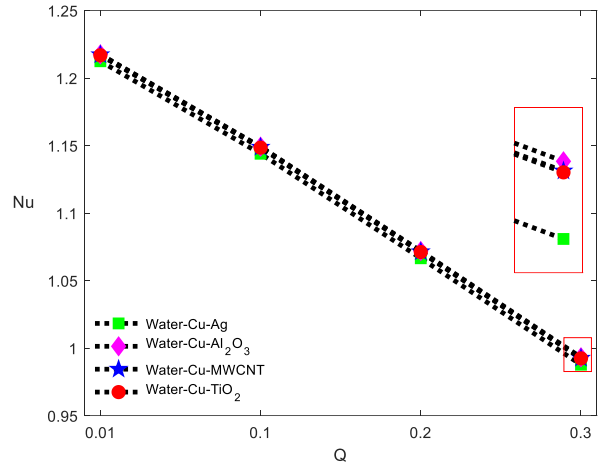

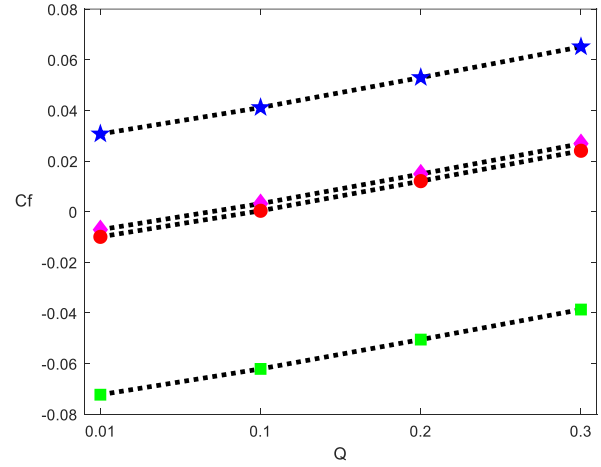

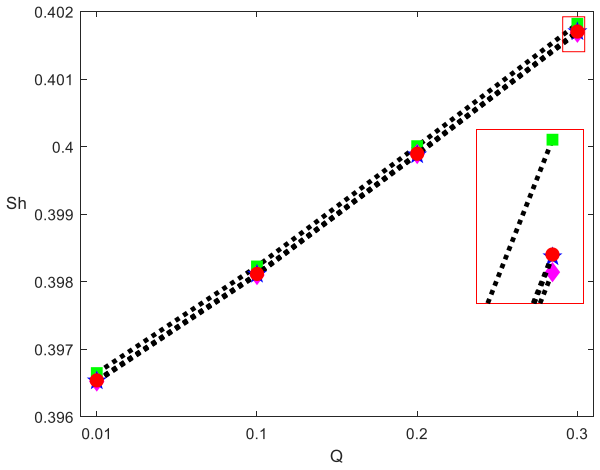

Fig. 24: Variation of Nu, Cf and Sh with respect to Q when $Gr = 5.0$, $Gc = 5.0$, $So = 0.1$, $Rn = 0.1$, $Du = 0.1$, $Da = 0.25$, $Q1 = 0.1$, $Ha = 2.5$, $Sc = 0.25$, $Ec = 0.1$, $\phi = 0.02$ and $Rd = 1$.

Nu, Cf, and Sh during the variation of Gc is similar to the variation in Gr. Still, there is an enhancement in Nu due to the improvement in Cf concerning the increment in Ω. Additionally, when $Gc = 2.5$, Cu-MWCNT-water HNF provides higher Nu, and Cu-Ag-water HNF provides lower Nu, similar to $Gr = 2.5$. However, when $Gc = 10.0$, Cu-Ag-water HNF provides higher Nu, and Cu-MWCNT-water HNF provides lesser Nu. Apart from this, an almost reverse distribution of Sh for HNFs is noted. It is observed that Cu-Al_2O_3-water HNF provides higher Nu and lower Sh when the mass Grashof number is set to 5.0 to 7.5. Until the mass Grashof number reaches $Gc = 7.5$, diffusive mass transfer decreases, and beyond $Gc = 7.5$, convection mass transfer increases. However, for every value of Gc, Cu-MWCNT-

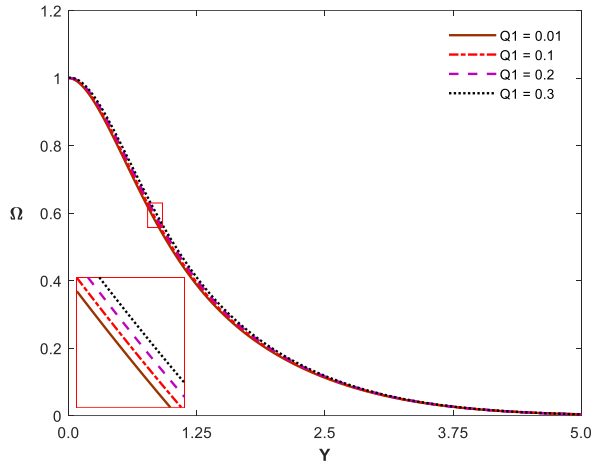

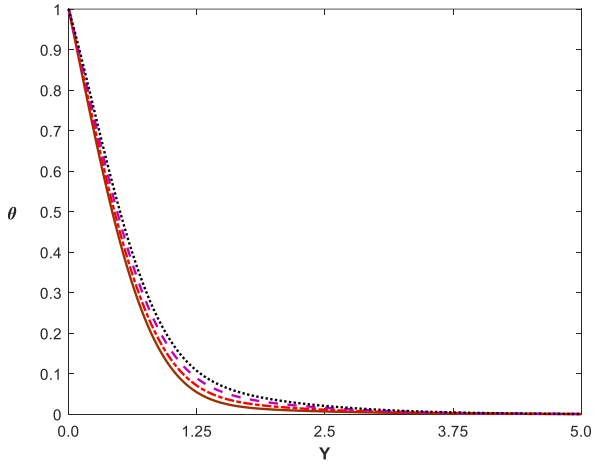

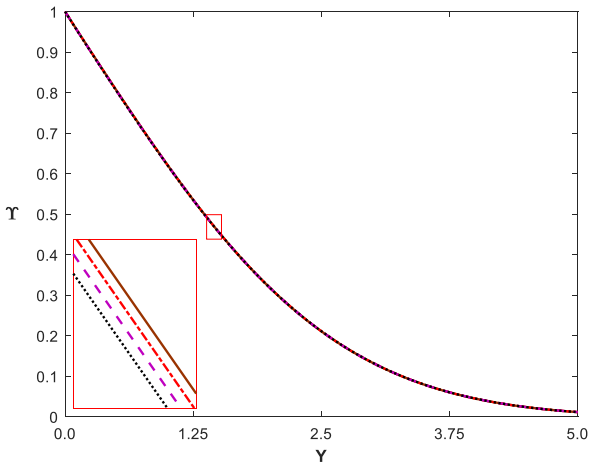

Fig. 25: Variation of Ω, θ and Υ with respect to $Q1$ when $Gr = 5.0$, $Gc = 5.0$, $So = 0.1$, $Rn = 0.1$, $Du = 0.1$, $Q = 0.1$, $Da = 0.25$, $Ha = 2.5$, $Sc = 0.25$, $Ec = 0.1$, $\phi = 0.02$ and $Rd = 1$.

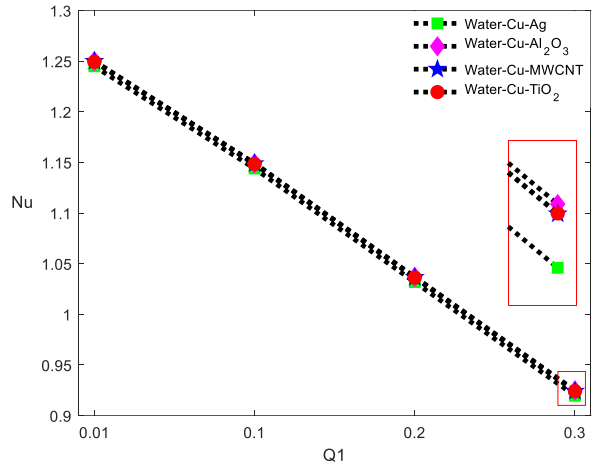

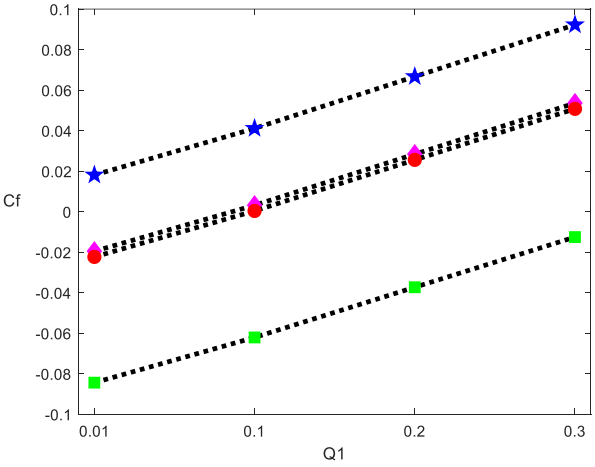

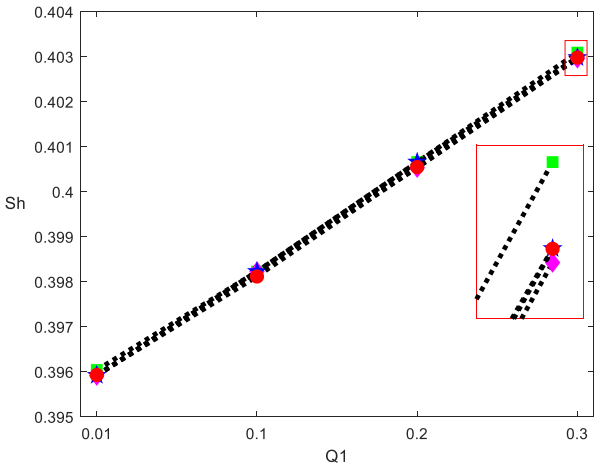

Fig. 26: Variation of Nu, Cf and Sh with respect to $Q1$ when $Gr = 5.0$, $Gc = 5.0$, $So = 0.1$, $Rn = 0.1$, $Du = 0.1$, $Q = 0.1$, $Da = 0.25$, $Ha = 2.5$, $Sc = 0.25$, $Ec = 0.1$, $\phi = 0.02$ and $Rd = 1$.

water HNF provides a higher range of Cf.

The effect of radiation on flow phenomenon and HMT by augmenting Rd to 0.1, 1.0, 2.0, and 3.0 is illustrated in Figs. 19 and 20. The figure is depicted when $Gr = 5.0$, $Da = 0.25$, $So = 0.1$, $Rn = 0.1$, $Du = 0.1$, $Q = 0.1$, $Q1 = 0.1$, $Ha = 2.5$, $Sc = 0.25$, $Ec = 0.1$, $\phi = 0.02$, and $Da = 0.25$. An increase in the value of Rd results in divergence from the boundary and convergence near the distance $Y = 2.0$. Moreover, until the distance of $Y = 2.5$, the temperature enhances with the radiation effect. This is due to the movement of heat energy in the form of electromagnetic waves directly from the source. Thus, the available energy causes the HNF to raise the temperature distribution to a certain distance based on the intensity from the source. It is

noted that Υ enhances with radiation up to $Rd = 2.0$, and on further increasing, there is a reduction in Υ. Under the convection-radiation effect, convection heat transfer increases with Rd, leading to a reduction in conduction heat transfer. Evidence of an increase in convection is observed with the rise in Cf. Along with Cf, mass transfer due to convection enhances with Rd. In the case of higher radiation effect ($Rd = 3.0$), Cu-Al_2O_3-water HNF delivers the highest range of Nu, and Cu-Ag-water HNF delivers the highest range of Sh. Compared to convection effects such as Gr and Gc, HNFs have a lesser effect with Rd.

The flow patterns with respect to changes in the first-order chemical reaction when $Gr = 5.0$, $Gc = 5.0$, $So = 0.1$, $Da = 0.25$, $Du = 0.1$, $Q = 0.1$, $Q1 = 0.1$, $Ha = 2.5$, $Sc = 0.25$, $Ec = 0.1$, $\phi = 0.02$, and $Rd = 1$ are illustrated in Figs. 21 and 22. The reaction parameter, Rn, where $Rn > 0$, illustrates the destructive mode of the concentration boundary layer, and if $Rn < 0$, the reaction will be constructive, leading to an improvement in the concentration boundary layer. Thus, an increase in Rn leads to a reduction in concentration. Furthermore, a reduction in concentration causes a decrease in velocity due to the reduction in buoyancy. Since both Ω and Υ are decreasing, skin friction also reduces. The Cf values, on increasing the Rn parameter, illustrate the reduction in the motion of HNF due to the destruction in the concentration boundary layer. Regarding Cf, there is a decrease in the heat transfer rate. However, there is a rise in diffusive mass transfer due to the flow restriction caused by the chemical reaction. Additionally, it is noticed that the Cu-Al_2O_3-water HNF delivers higher heat transfer, while Cu-Ag-water HNF delivers lower heat transfer. A reverse trend is noticed in the Sh plot. Moreover, similar to the previous results, Cu-MWCNT-water HNF has a higher flow motion capacity, providing a higher Cf.

The effect of heat source/heat generation on HNF flow over a vertical plate is identified and depicted in Figs. 23 and 24. The HNF flow and HMT plots are visualized when $Gr = 5.0$, $Gc = 5.0$, $So = 0.1$, $Rn = 0.1$, $Du = 0.1$, $Da = 0.25$, $Q1 = 0.1$, $Ha = 2.5$, $Sc = 0.25$, $Ec = 0.1$, $\phi = 0.02$, and $Rd = 1$. Thermal energy is built up from another source of energy and involves the modification of the flow field. Thus, there is a surge in θ, and this interrelates to Ω and Υ, enhancing them as well. The thermal energy surges to create convection with respect to the improvement in flow motion. Furthermore, there is a reduction in conduction behavior by increasing the value of Q. This reduction in conduction is due to the surge in convection behavior due to heat generation. A small rise in Cf is noted because of the improvement in HNF flow motion. In relation to this, there is an alteration in the boundary layer, leading to a change in the convection mass transfer rate. Additionally, it is noted that Cu-Ag-water HNF provides a higher Sh followed by Cu-TiO_2-water HNF, Cu-MWCNT-water HNF, and Cu-Al_2O_3-water HNF. This is the reverse order of higher Nu.

Since all liquids and solids absorb radiation, the effect of the radiation absorption parameter on HMT and other flow behaviors is illustrated in Figs. 25 and 26 when choosing other non-dimensional parameters as $Gr = 5.0$, $Gc = 5.0$, $So = 0.1$, $Rn = 0.1$, $Du = 0.1$, $Q = 0.1$, $Da = 0.25$, $Ha = 2.5$, $Sc = 0.25$, $Ec = 0.1$, $\phi = 0.02$, and $Rd = 1$

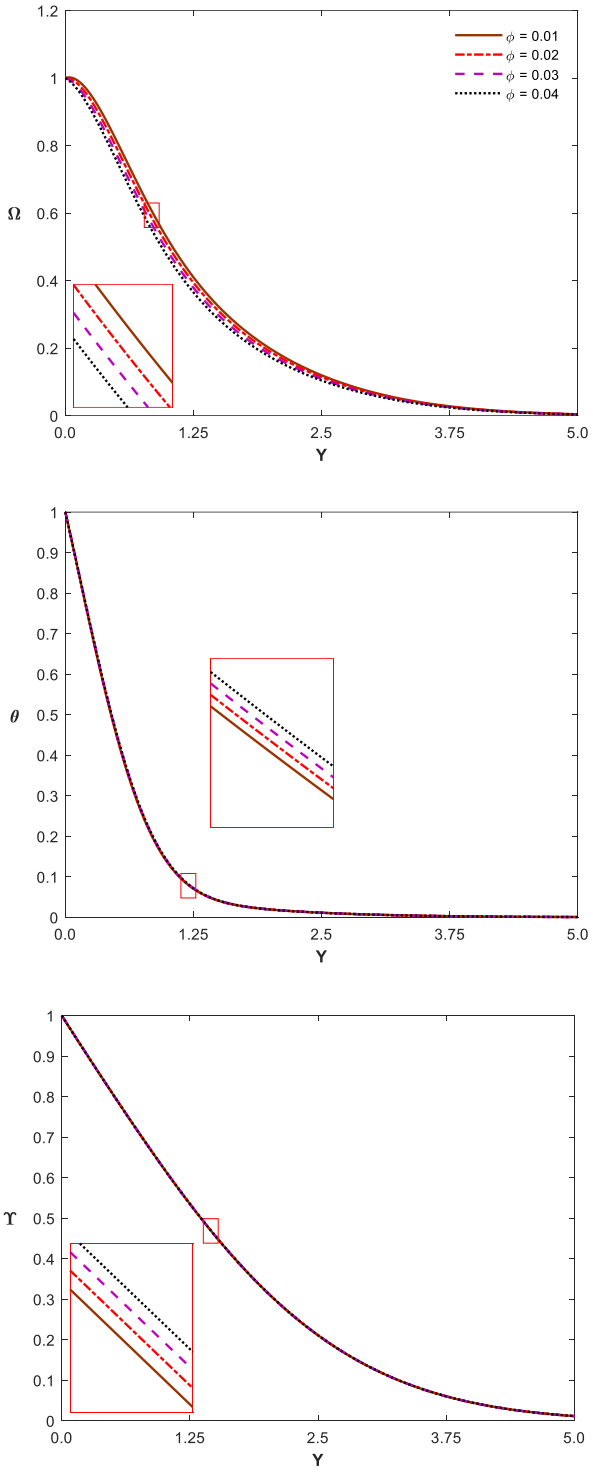

Fig. 27: Variation of Ω, θ and Υ with respect to ϕ when $Gr = 5.0$, $Gc = 5.0$, $So = 0.1$, $Rn = 0.1$, $Du = 0.1$, $Q = 0.1$, $Q1 = 0.1$, $Ha = 2.5$, $Sc = 0.25$, $Ec = 0.1$, $Da = 0.25$ and $Rd = 1$.

respectively. The conversion of electromagnetic radiation effects to internal energy is developed when the effects of radiation absorption are included. An increase in the value of $Q1$ leads to a correction in the buoyancy force and makes Ω rise. This buoyancy force causes an improvement in flow motion and carries energy within the fluid to a long distance. Thus, there is an enhancement in θ. However, a fall in

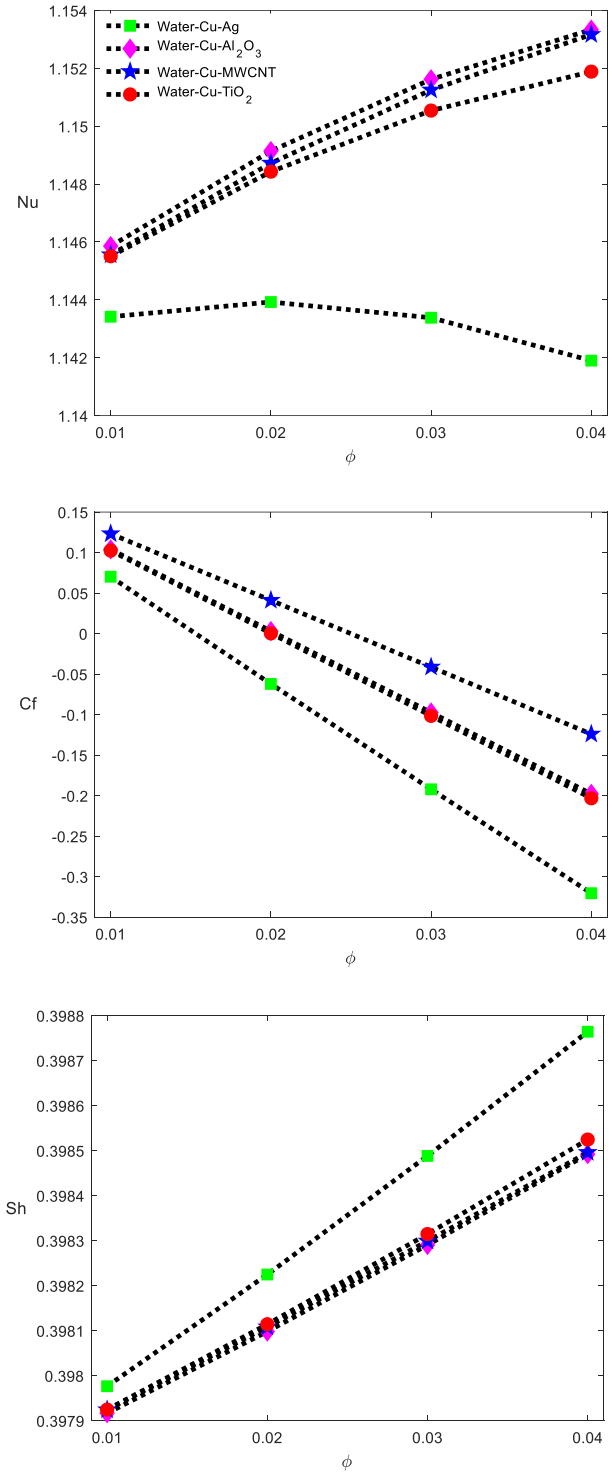

Fig. 28: Variation of Nu, Cf and Sh with respect to ϕ when $Gr = 5.0$, $Gc = 5.0$, $So = 0.1$, $Rn = 0.1$, $Du = 0.1$, $Q = 0.1$, $Q1 = 0.1$, $Ha = 2.5$, $Sc = 0.25$, $Ec = 0.1$, $Da = 0.25$ and $Rd = 1$.

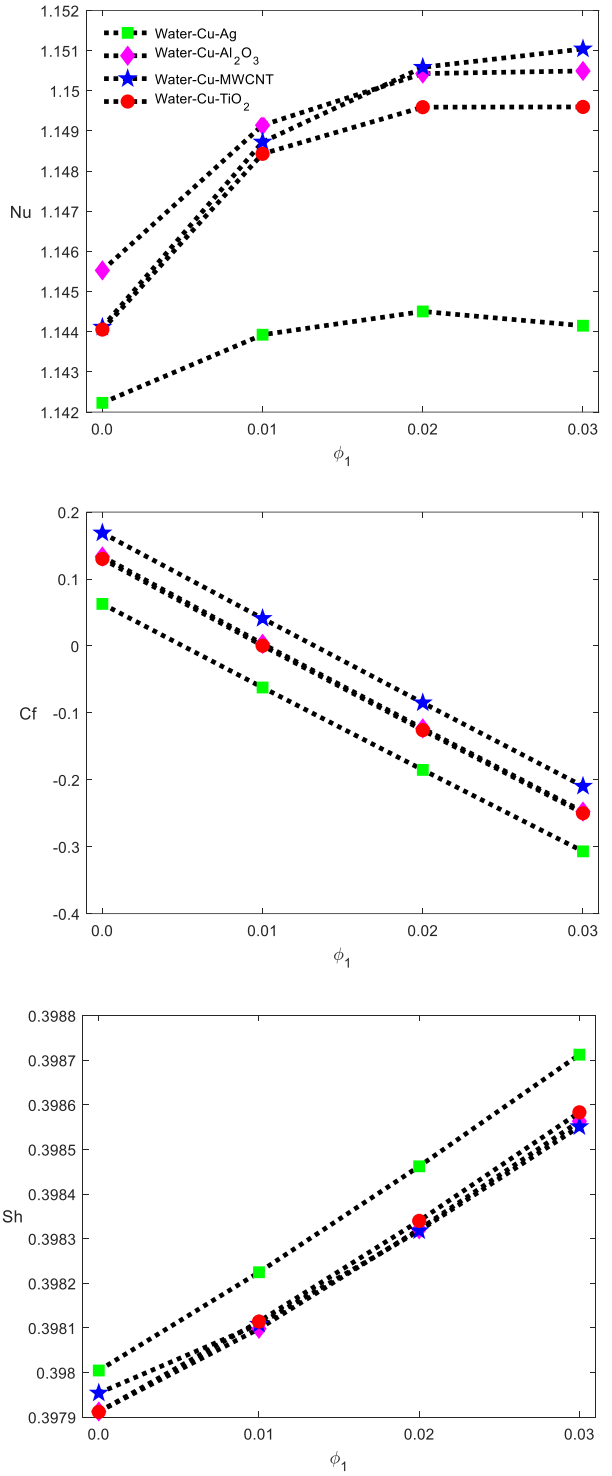

Fig. 29: Variation of Ω, θ and Υ with respect to ϕ_1 with fixed $\phi_2 = 0.01$.

Υ is noticed with $Q1$. With respect to flow motion and the buoyancy effect, Cf improves with $Q1$. In addition, an advancement in Sh and a reduction in Nu are noted. This illustrates the reduction in conduction-based heat transfer and a surge in convection-based mass transfer.

The inclusion of hybrid nanoparticles on HMT is represented in Figs. 27-30. The flow results are plotted when $Gr = 5.0$, $Gc = 5.0$, $So = 0.1$, $Rn = 0.1$, $Du = 0.1$, $Q = 0.1$, $Q1 = 0.1$, $Ha = 2.5$, $Sc = 0.25$, $Ec = 0.1$, $Da = 0.25$, and $Rd = 1$. It is detected that there is a fall in Ω when increasing the value of ϕ. The results are spotted in Figs 27 and 28 by considering $\phi_1 = \phi_2$ (when $\phi = 0.03$, $\phi_1 = 0.015$, and $\phi_2 = 0.015$). The reduction in Ω is mainly due to the enhancement in density by the summation of additional hybrid nanoparticles. The viscosity of the running fluid raises and makes the fluid heavier.

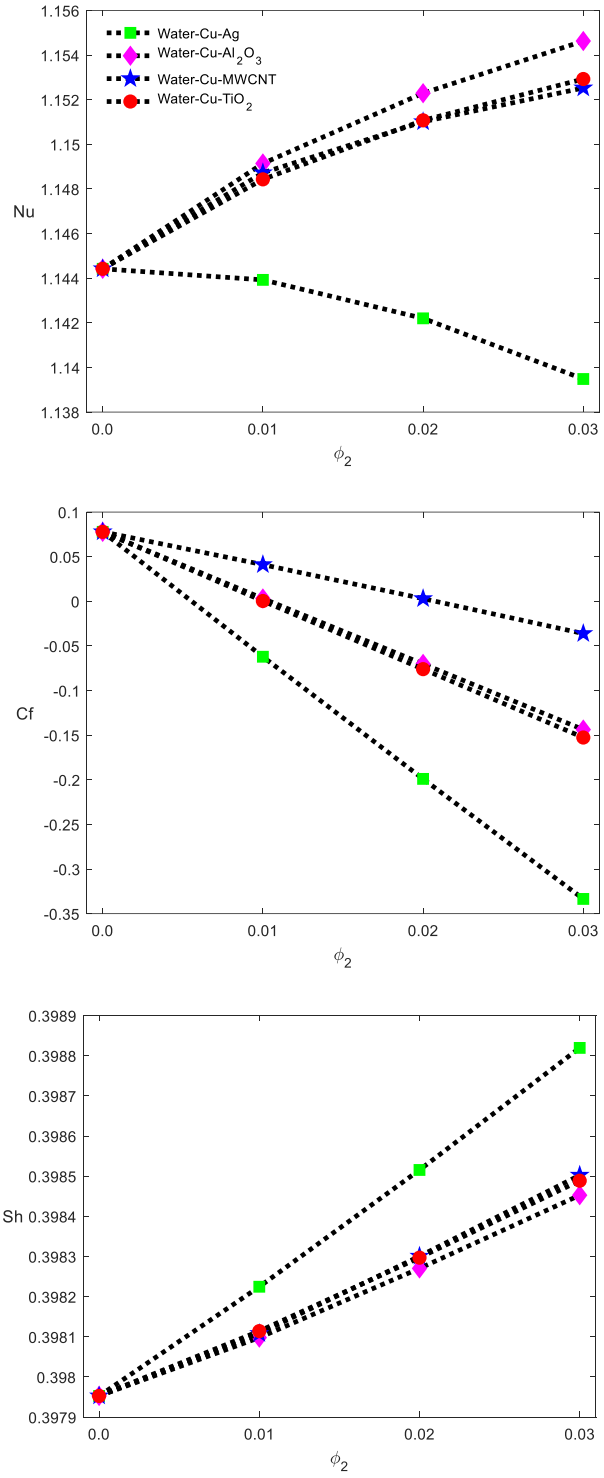

Fig. 30: Variation of Ω, θ and Υ with respect to ϕ_2 with fixed $\phi_1 = 0.01$.

However, the distribution of θ and Υ improves with ϕ. This is because of the incorporation of thermophysical properties when adding the hybrid nanoparticles. In the case of the Nu plot, there is a continuous hike in Nu when considering Cu-Al_2O_3-water, Cu-MWCNT-water, and Cu-TiO_2-water HNF as a running fluid. However, when considering Cu-Ag-water HNF as a running fluid, there is a fall noticed after a rise. There is only a continuous Cf spotted for every HNF. This, in turn, illustrates the shoot-up in heat transfer effect with the addition of ϕ. But, the improvement of Nu is because of the thermophysical property of every nanoparticle addition. Apart from this, there is a continuous rise in Sh spotted, and this illustrates that the addition of ϕ leads to an enhancement of the diffusive mass transfer rate. While considering fixed ϕ_1 and changing ϕ_2 (Fig. 29), heat transfer by Cu-Al_2O_3-water is higher when $\phi_1 < 0.02$ and heat transfer by Cu-MWCNT-water hybrid nanofluid is higher when $\phi_1 > 0.02$. However, while considering fixed ϕ_2 and changing ϕ_1 (Fig. 30), heat transfer by Cu-Al_2O_3-water hybrid nanofluid is greater than other hybrid nanofluid. In addition to this, it is found that the skin friction by Cu-MWCNT-water hybrid nanofluid is always higher while increasing ϕ_1 and ϕ_2.

V. Conclusion

The study is carried out to explore the radiative-MHD free convection flow phenomenon and heat transfer (HMT) effects when hybrid nanofluids (HNF) pass a vertical plate under a porous medium. Additionally, a comparison of HMT rates of various Cu-water-based hybrid nanoliquids is analyzed. The important findings from the study, considering viscous dissipation, heat source, radiation absorption, and chemical reaction effects, are as follows:

- An increase in Da leads to clearer permeability and allows the HNF to flow freely. This free flow also reduces conduction-based heat transfer.
- At higher Da, Al_2O_3-Cu-water HNF provides higher Nu and lower Sh; MWCNT-Cu-water HNF provides lower Nu but higher Cf and Sh; Ag-Cu-water HNF provides lower Cf.
- The flow of Al_2O_3-Cu-water HNF is enhanced with an increase in the Eckert number, radiation parameter, Dufort and Soret numbers, thermal and mass Grashof numbers, heat source, and radiation absorption parameter. Meanwhile, an increase in reaction parameter, Schmidt number, magnetic parameter, and volume fraction of hybrid nanoparticles leads to a reduction in HNF flow velocity.
- Temperature distribution has a more significant response to radiation and radiation absorption parameters, while other effects have fewer responses.
- Concentration distribution improves with permeability, Eckert number, magnetic parameter, Soret number, thermal Grashof number, heat source parameter, and the volume fraction of HP.
- Convection-based heat transfer increases with permeability, Eckert number, Dufort number, Soret number, thermal and mass Grashof numbers, radiation parameter, heat source, and radiation absorption parameter.
- In general, Al_2O_3-Cu-water HNF provides a higher heat transfer rate. However, under higher viscous dissipation and magnetic field effects, MWCNT-Cu-water HNF provides higher Nu. Also, at higher values of mass Grashof number, Ag-Cu-water HNF provides higher Nu.
- In general, skin friction is found to be higher for MWCNT-Cu-water HNF and lower for Ag-Cu-water HNF. Also, Sh is greater for Ag-Cu-water HNF. However, when thermal and mass Grashof numbers increase, Sh is higher for MWCNT-Cu-water HNF.

REFERENCES

[1] S. Kakac, W. Aung, and R. Viskanta, *Natural Convection: Fundamentals and Applications*, 1985.

[2] F. P. Incropera, "Convection heat transfer in electronic equipment cooling," *Journal of Heat Transfer*, vol. 110, no. 4, pp1097–1112, 1988.

[3] M. Kaviany, *Principles of Heat Transfer in Porous Media*. Springer, 1995.

[4] T. L. Bergman, T. L. Bergman, F. P. Incropera, D. P. DeWitt, and A. S. Lavine, *Fundamentals of Heat and Mass Transfer*. Wiley, 2011.

[5] Y. Jaluria, "Heat and mass transfer in materials processing and manufacturing," *Advances in Heat Transfer*, vol. 48, pp1–94, 2016.

[6] E. M. Sparrow and K. K. Tien, "Forced convection heat transfer at an inclined and yawed square plate — application to solar collectors," *Journal of Heat Transfer*, vol. 99, no. 4, pp507–512, 1977.

[7] L. T. Yeh, "Review of heat transfer technologies in electronic equipment," *Journal of Electronic Packaging*, vol. 117, no. 4, pp333–339, 1995.

[8] E. Rezaei, M. Barbato, S. Gianella, A. Ortona, and S. Haussener, "Pressure drop and convective heat transfer in different sisic structures fabricated by indirect additive manufacturing," *Journal of Heat Transfer*, vol. 142, no. 3, pp32 702–32 710, 2020.

[9] J. Lawrence, B. Mohanadhas, N. Narayanan, A. V. Kumar, V. Mangottiri, and S. K. Govindarajan, "Numerical modelling of nitrate transport in fractured porous media under non-isothermal conditions," *Environmental Science and Pollution Research*, vol. 29, no. 10, pp85 922–85 944, 2022.

[10] J. Lawrence, V. K. Alagarsamy, B. Mohanadhas, N. Natarajan, M. Vasudevan, and S. K. Govindarajan, "Nitrate transport in a fracture-skin-matrix system under non-isothermal conditions," *Environmental Science and Pollution Research*, vol. 30, no. 7, pp18 091–18 112, 2023.

[11] V. M. Soundalgekar, "Free convection effects on the stokes problem for an infinite vertical plate," *Journal of Heat Transfer*, vol. 99, no. 3, pp499–501, 1977.

[12] N. G. Kafoussias, "Mhd thermal-diffusion effects on free-convective and mass-transfer flow over an infinite vertical moving plate," *Astrophysics and Space Science*, vol. 192, no. 1, pp11–19, 1992.

[13] M. A. Hossain, K. Khanafer, and K. Vafai, "The effect of radiation on free convection flow of fluid with variable viscosity from a porous vertical plate," *International Journal of Thermal Sciences*, vol. 40, no. 2, pp115–124, 2001.

[14] R. Muthucumaraswamy, "Chemical reaction effects on vertical oscillating plate with variable temperature," *Chemical Industry and Chemical Engineering Quarterly*, vol. 16, no. 2, pp167–173, 2010.

[15] M. Ghani, T. Utomo, Y. Norasia, and D. S. Mukama, "Fluid dynamics of free convection flow in unsteady state over single inclined flat plate," *IAENG International Journal of Computer Science*, vol. 50, no. 2, pp620–632, 2023.

[16] Q. Rubbab, D. Vieru, C. Fetecau, and C. Fetecau, "Natural convection flow near a vertical plate that applies a shear stress to a viscous fluid," *PLoS One*, vol. 8, no. 11, pp1–7, 2013.

[17] T. R. Rani and R. Palli, "Mhd free convective heat transfer flow past vertical plate embedded in a porous medium with effects of variable fluid properties in the presence of heat source," *Lecture Notes in Engineering and Computer Science*, vol. 2, pp1262–1267, 2014.

[18] A. Ahmed, M. N. Sarki, and M. Ahmad, "Radiation effects on heat and mass transfer over an exponentially accelerated infinite vertical plate with chemical reaction," *Lecture Notes in Engineering and Computer Science*, vol. 2210, pp10–15, 2014.

[19] M. Umamaheswar, S. V. K. Varma, and M. C. Raju, "Unsteady mhd free convective visco-elastic fluid flow bounded by an infinite inclined porous plate in the presence of heat source, viscous dissipation and ohmic heating," *International Journal of Advanced Science and Technology*, vol. 61, pp39–52, 2013.

[20] C. Y. Cheng, "Mixed convection heat transfer from a vertical plate embedded in a bidisperse porous medium," *Lecture Notes in Engineering and Computer Science*, vol. 2218, pp1330–1335, 2015.

[21] R. Seshadri and S. R. Munjam, "Mixed convection flow due to a vertical plate in the presence of heat source and chemical reaction," *Ain Shams Engineering Journal*, vol. 7, no. 2, pp671–682, 2016.

[22] T. M. Agbaje, S. S. Motsa, P. Leach, and P. Sibanda, "Efficient large spectral collocation method for mhd laminar natural convection flow from a vertical permeable flat plate with uniform surface temperature, soret, dufour, chemical reaction and thermal radiation," *IAENG International Journal of Applied Mathematics*, vol. 50, no. 3, pp490–504, 2020.

[23] S. T. Suganya, P. Balaganesan, L. Rajendran, and M. Abukhaled, "Analytical discussion and sensitivity analysis of parameters of magnetohydrodynamic free convective flow in an inclined plate," *European Journal of Pure and Applied Mathematics*, vol. 13, no. 3, pp631–644, 2020.

[24] A. A. G. Aravind and J. Ravikumar, "Effects of thermal radiation in a rotating fluid on an oscillating vertical plate with variable temperature and mass diffusion," *IAENG International Journal of Applied Mathematics*, vol. 54, no. 1, pp128–139, 2024.

[25] S. U. S. Choi and J. A. Eastman, "Enhancing thermal conductivity of fluids with nanoparticles," in *ASME International Mechanical Engineering Congress and Exposition*, 1995.

[26] M. S. Kandelousi, *Nanofluid Heat and Mass Transfer in Engineering Problems*. InTech, 2017.

[27] L. Jino and A. V. Kumar, "Fluid flow and heat transfer analysis of quadratic free convection in a nanofluid filled porous cavity," *International Journal of Heat and Technology*, vol. 39, no. 3, pp876–884, 2021.

[28] A. V. Kumar, J. Lawrence, and G. Saravanakumar, "Fluid friction/heat transfer irreversibility and heat function study on mhd free convection within the mwcnt–water nanofluid-filled porous cavity," *Heat Transfer*, vol. 51, no. 5, pp4247–4267, July 2022.

[29] C. Ramreddy, P. V. S. N. Murthy, A. J. Chamkha, and A. M. Rashad, "Soret effect on mixed convection flow in a nanofluid under convective boundary condition," *International Journal of Heat and Mass Transfer*, vol. 64, pp384–392, 2013.

[30] F. Ali, M. Gohar, and I. Khan, "Mhd flow of water-based brinkman type nanofluid over a vertical plate embedded in a porous medium with variable surface velocity, temperature and concentration," *Journal of Molecular Liquids*, vol. 223, pp412–419, 2016.

[31] H. T. Alkasasbeh, M. Z. Swalmeh, A. Hussanan, and M. Mamat, "Numerical solution of heat transfer flow in micropolar nanofluids with oxide nanoparticles in water and kerosene oil about a horizontal circular cylinder," *IAENG International Journal of Applied Mathematics*, vol. 49, no. 3 pp326–333, 2019.

[32] P. C. Reddy, M. C. Raju, and G. S. S. Raju, "Free convective heat and mass transfer flow of heat-generating nanofluid past a vertical moving porous plate in a conducting field," *Special Topics Reviews in Porous Media*, vol. 7, no. 2, pp161–180, 2016.

[33] B. O. Falodun and F. D. Ayegbusi, "Soret–dufour mechanism on an electrically conducting nanofluid flow past a semi-infinite porous plate with buoyancy force and chemical reaction influence," *Numerical Methods for Partial Differential Equations*, vol. 37, no. 2, pp1419–1438, 2021.

[34] N. Khan, F. Ali, M. Arif, Z. Ahmad, A. Aamina, and I. Khan, "Maxwell nanofluid flow over an infinite vertical plate with ramped and isothermal wall temperature and concentration," *Mathematical Problems in Engineering*, vol. 2021, pp1–19, 2021.

[35] S. Arulmozhi, K. Sukkiramathi, S. S. Santra, R. Edwan, U. Fernandez-Gamiz, and S. Noeiaghdam, "Heat and mass transfer analysis of radiative and chemical reactive effects on mhd nanofluid over an infinite moving vertical plate," *Results in Engineering*, vol. 14, pp100 394–100 402, 2022.

[36] J. Lawrence, K. V. Rajadren, S. Doley, V. K. Alagarsamy, A. Jacob, and B. Mohanadhas, "Nanoparticles: an overview," in *Green Magnetic Nanoparticles (GMNPs)*. Elsevier, 2024, pp3–21.

[37] S. Suresh, K. P. Venkitaraj, P. Selvakumar, and M. Chandrasekar, "Synthesis of al$_2$o$_3$–cu/water hybrid nanofluids using two step method and its thermo physical properties," *Colloids and Surfaces A: Physicochemical and Engineering Aspects*, vol. 388, no. 1, pp41–48, 2011.

[38] H. M. Ali, *Hybrid Nanofluids for Convection Heat Transfer*. Academic Press, 2020.

[39] L. Jino and A. V. Kumar, "Mhd natural convection of hybrid nanofluid in a porous cavity heated with a sinusoidal temperature distribution," *Computational Thermal Sciences: An International Journal*, vol. 13, no. 5, pp83–99, 2021.

[40] S. Doley, A. V. Kumar, and L. Jino, "Time fractional transient magnetohydrodynamic natural convection of hybrid nanofluid flow over an impulsively started vertical plate," *Computational Thermal Sciences: An International Journal*, vol. 14, no. 3, pp59–82, 2022.

[41] A. Bibi, H. Xu, Q. Sun, I. Pop, and Q. Zhao, "Free convection of a hybrid nanofluid past a vertical plate embedded in a porous medium with anisotropic permeability," *International Journal of Numerical Methods for Heat & Fluid Flow*, vol. 22, no. 7, pp4083–4101, 2020.

[42] V. Rajesh, M. A. Sheremet, and H. F. Öztop, "Impact of hybrid nanofluids on mhd flow and heat transfer near a vertical plate with ramped wall temperature," *Case Studies in Thermal Engineering*, vol. 28, pp101 557–101 572, 2021.

[43] N. S. Wahid, N. M. Arifin, N. S. Khashi'ie, I. Pop, N. Bachok, and M. E. H. Hafidzuddin, "Hybrid nanofluid radiative mixed convection stagnation point flow past a vertical flat plate with dufour and soret effects," *Mathematics*, vol. 10, no. 16, pp1–24, 2022.

[44] B. Jaismitha and J. Sasikumar, "Chemically reactive oscillatory casson hybrid nanofluid flow with heat generation/absorption phenomenon

through radiating wavy channel," *IAENG International Journal of Applied Mathematics*, vol. 53, no. 4, pp1148–1161, 2023.

[45] P. Gumber, M. Yaseen, S. K. Rawat, and M. Kumar, "Heat transfer in micropolar hybrid nanofluid flow past a vertical plate in the presence of thermal radiation and suction/injection effects," *Partial Differential Equations in Applied Mathematics*, vol. 5p.100240, 2022.

[46] S. Doley, A. V. Kumar, K. S. Singh, and L. Jino, "Study of time fractional burgers' equation using fractional derivatives," *Engineering Letters*, vol. 30, no. 3, pp1017–1024, 2023.

[47] R. Muthucumaraswamy, P. Ganesan, and V. M. Soundalgekar, "Heat and mass transfer effects on flow past an impulsively started vertical plate," *Acta Mechanica*, vol. 146, no. 1, pp1–8, 2001.